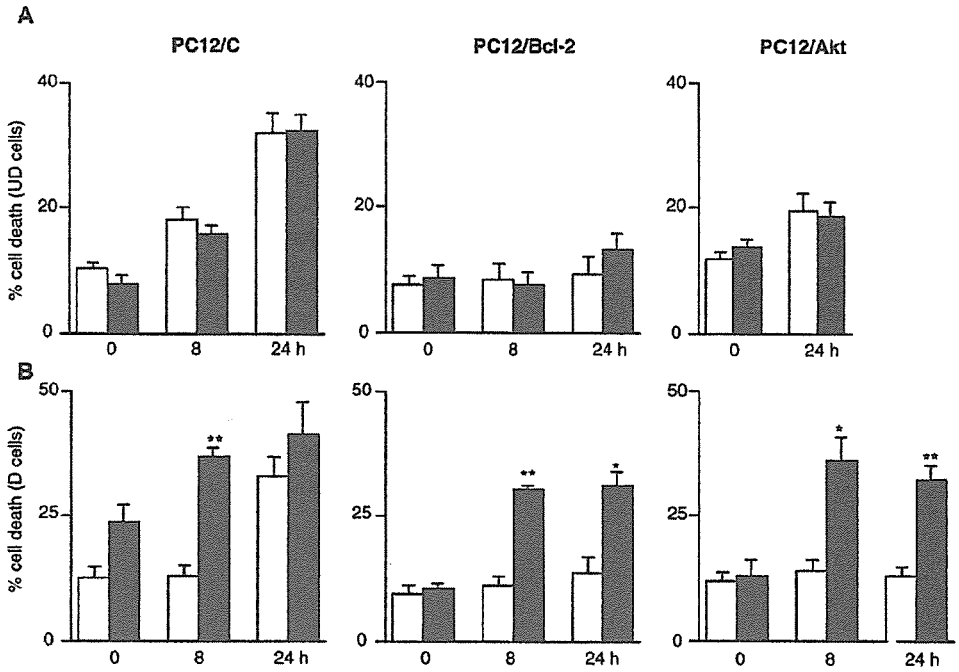

FIG. 6. **Transient co-transfection of PC12 cells with GFP plus Ub-ΔN-AVPI or MVPI Smac/DIABLO.** *A*, undifferentiated PC12/C, PC12/Bcl-2, and PC12/Akt cells were co-transfected with pEGFP and either Ub-ΔN-AVPI (*solid square*) or Ub-ΔN-MVPI (*open square*) Smac/DIABLO. Cell death was quantified in the presence of serum (0 h) and after 8 and 24 h of serum deprivation. The results are mean ± S.E. (n = 3). *B*, results of cell death following co-transfection with Ub-ΔN-AVPI (■) or Ub-ΔN-MVPI (□) Smac/DIABLO in differentiated PC12/C, PC12/Bcl-2, and PC12/Akt containing NGF/Bt_2cAMP (0 h) and after withdrawal of NGF/Bt_2cAMP for 8 and 24 h. The results are mean ± S.E. (n = 3). *, $p < 0.05$; **, < 0.01; in Ub-ΔN-AVPI *versus* Ub-ΔN-MVPI transfected cells (Student's t test, two-tailed).

differentiated cells, in differentiated PC12 cells, Bcl-2 and activated Akt also inhibit the subsequent activation of caspase 9. Further analysis concerning regulation of the caspase 9 pathway by Smac/DIABLO and XIAP indicate that in differentiated but not undifferentiated cells, the IAP binding motif of Smac/DIABLO plays an important role in activating caspase 9 pathway, most likely, by alleviating IAP inhibition. These results strongly suggest that the PC12 differentiation program alters regulation of events downstream of mitochondrial release of apoptogenic factors.

Release of hcC, Smac/DIABLO, and Omi/HtrA2 from Mitochondria in Factor-deprived PC12 Cells—In cell death induced by trophic factor deprivation, we observed high cytosolic hcC levels in both undifferentiated and NGF/Bt_2cAMP-differentiated PC12 cells. In addition to hcC, the processed forms of both Smac/DIABLO and Omi/HtrA2 were also released from mitochondria during factor-deprivation in PC12 cells. The kinetic analysis revealed an early cytosolic accumulation of these proteins, already evident by 4 h of factor deprivation. However, the peak DEVD cleaving activity occurred at around 16 h (data not shown) just preceding cell death. Because we observed a significant delay before caspases were activated, even though these proteins are released rapidly from mitochondria, this indicates mitochondrial release of these factors is not the rate-limiting event for apoptosis. This result is in accordance with previous findings that, although release of hcC from mitochondria is a critical early event in caspase activation, it does not coincide with the commitment point to cell death (32, 41). Moreover, in response to apoptotic signals such as factor withdrawal, cells can withstand high cytosolic hcC levels and survive as long as caspase activation is inhibited and mitochondrial function maintained (30, 42). Other factors, for example, attainment of optimal cytoplasmic levels of these released proteins, may also play a role in determining the activation of the caspase 9 cascade. In this respect, the kinetic data show that in undifferentiated PC12/Bcl-2 and PC12/Akt cells, the release of hcC is less than in PC12/C cells.

The mature Smac/DIABLO and Omi/HtrA2 proteins have an exposed tetrapeptide IAP-binding motif (IBM) at the N terminus, which by binding to XIAP, c-IAP-1, or c-IAP-2 abrogates IAP inhibition of caspase 9 and the effectors caspases 3 and 7, resulting in positive amplification of caspase loop (34). Co-release of these proteins with hcC in factor-deprived PC12 cells suggests that the inhibitors such as IAPs are removed from caspases allowing them to function in cellular demise. The removal may involve degradation of IAPs as shown in the case of XIAP by Omi/HtrA2 (43). In this regard, we find that XIAP levels decrease in differentiated PC12/C cells deprived of trophic support. Omi/HtrA2 may have other targets. For example, the serine protease inhibitor 4-(2-aminoethyl)benzenesulfonyl fluoride hydrochloride was shown to inhibit cleavage of c-IAP-1 by Omi/HtrA2 (44). 4-(2-Aminoethyl)benzenesulfonyl fluoride hydrochloride has also been reported to inhibit caspase 2 processing and cell death in trophic-deprived PC12 cells (45). It is probable that the released Omi/HtrA2 that we observe activates caspase 2, because caspase 2 is cleaved after serum or NGF/Bt_2cAMP withdrawal in undifferentiated and differentiated cells, respectively (data not shown). In differentiated and undifferentiated PC12 cells, the release of mitochondrial hcC, as well as of Smac/DIABLO was suppressed by Bcl-2 or constitutively active Akt. Suppression of Smac/DIABLO release by Bcl-2 and Akt presumably damps down a feed-forward mitochondrial amplification loop ensuring that caspases are not activated. Reinforcing this proposition are the results showing that differentiated PC12/Bcl-2 and PC12/Akt cells are sensitive to Ub-ΔN-AVPI-Smac/DIABLO. We observed that the inhibitory effect of Bcl-2 or Akt on mitochondrial release extended for a longer period in differentiated cells compared with undifferentiated PC12 cells. This observation suggests

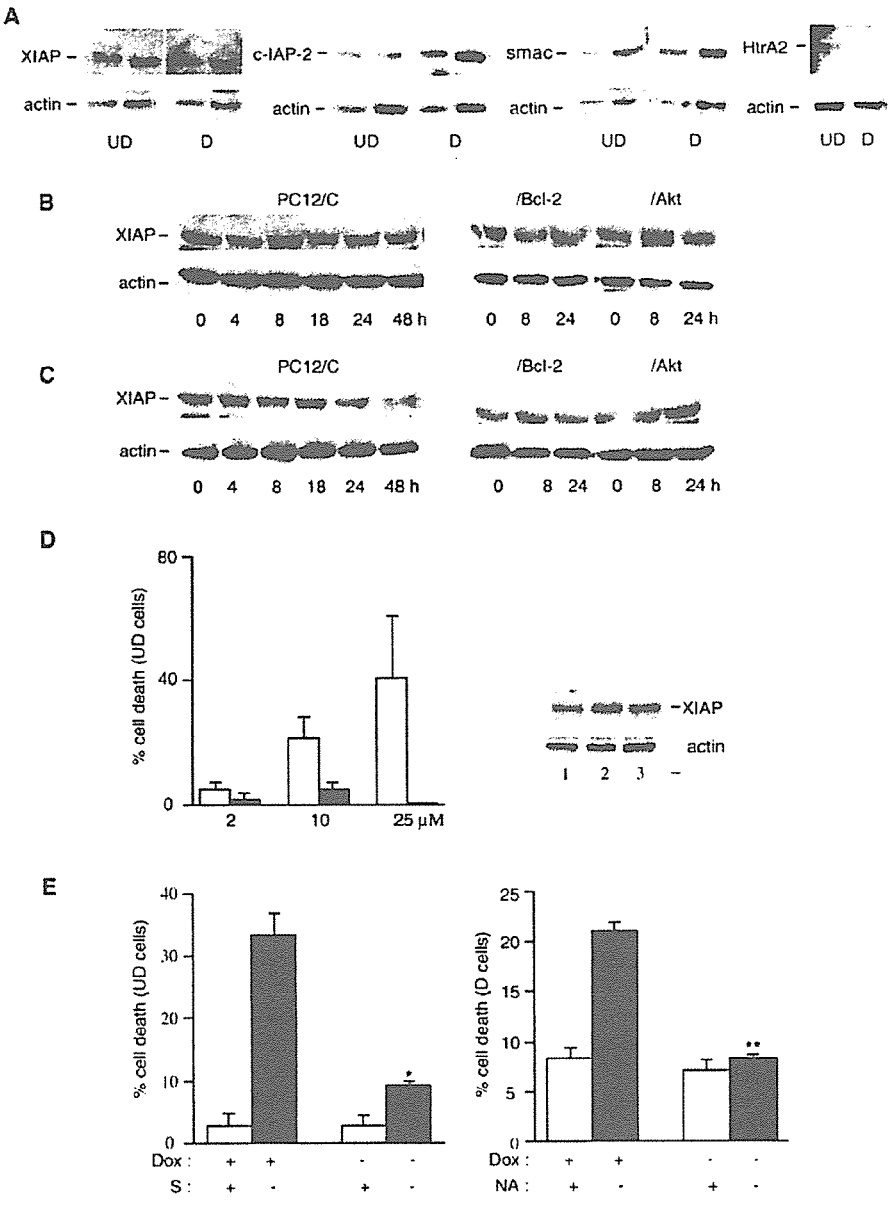

FIG. 7. **Acquisition of IAP regulation of cell death in differentiated cells.** *A*, XIAP, c-IAP-2, Smac, and htrA2 levels were analyzed in undifferentiated (*UD*) and differentiated (*D*) cells using 10 and 20 μg of total protein for XIAP, c-IAP-2, and Smac; and 20 μg for HtrA2. The blots were also analyzed for actin levels. Results were quantified and corrected for protein levels. There is an increase in c-IAP-2 level in differentiated cells. *B*, XIAP levels in undifferentiated PC12/C, PC12/Bcl-2, and PC12/Akt cells following withdrawal of serum. 50 μg of total protein was used, and the same blots were analyzed for actin levels as control for protein loading. *C*, XIAP levels in differentiated PC12/C, PC12/Bcl-2, and PC12/Akt cells containing NGF/Bt_2cAMP (0 h) and following withdrawal of NGF/Bt_2cAMP at times indicated. *D*, microinjection of cytochrome *c* in XIAP-tetracycline-repressible undifferentiated PC12/C cells. The cells were co-microinjected with rhodamine and concentrations of cytochrome *c* as shown, in the presence (*open square*) and in the absence (*solid square*) of doxycycline. Cell death was analyzed 6 h later and quantified. Each experiment was done in duplicate, and the results are expressed as mean ± S.D., $n = 2$–3. *Right panels*: analysis of XIAP protein in PC12/C (*1*) and in PC12/XIAP cells, in the absence (*2*) and presence (*3*) of doxycycline. *E*, cell death following withdrawal of trophic support in XIAP-tetracycline repressible undifferentiated (*UD*) and differentiated (*D*) PC12 cells. Cell death was analyzed in cells containing doxycycline in the presence and absence of serum (*S*) in undifferentiated cells or NGF/Bt_2cAMP (*NA*) in differentiated cells. Doxycycline was withdrawn for about 16 h prior to testing cell death in the presence or absence trophic support. The results are expressed as mean ± S.E., $n = 4$. *, $p < 0.05$; **, $p < 0.001$; in the presence of doxycycline *versus* in the absence of doxycycline.

that differentiation has possibly modulated processes, which are involved in translocating these proteins from mitochondria to cytoplasm, and that control at this level is more stringent in differentiated cells.

Regulation of Cell Death Post-hcC Release from Mitochondria—Directly introducing cytochrome *c* into PC12 cells by microinjection triggers apoptosis. Such apoptosis must involve activation of caspase 9 for the following reasons: First, the ability of cytoplasmic extracts to induce *in vitro* processing of procaspase 9 mirrored cell death that was observed with microinjected cytochrome *c*. Second, endogenous procaspase 9 was cleaved in trophic factor-deprived cells. Third, cell death was suppressed by expression of a dominant negative caspase 9 mutant. Caspase 9 is activated when holocytochrome c, translocated from mitochondria, induces oligomerization of Apaf-1, a process dependent on ATP (16, 46, 47). Procaspase 9, which is either already associated with Apaf-1 as a holoenzyme (16) or recruited following hcC release, is then cleaved and activated within this "apoptosome complex."

Undifferentiated PC12 cells exhibited markedly greater sensitivity to induction of apoptosis by microinjected cytochrome *c* than differentiated cells. Additionally, NGF, Bcl-2, or constitutively active Akt were ineffective in protecting undifferentiated PC12 cells against microinjected cytochrome *c*. The greater sensitivity cannot simply be explained by differences in surface area (differentiated cells have approximately 1.5× greater surface area) as microinjections of even low concentrations of cytochrome *c* induced cell death that was not inhibited by anti-apoptotic factors. In sharp contrast, resistance to microinjected cytochrome *c* was found in differentiated PC12 cells; there are a delay period before cell death occurred indicating that the differentiation process enables the cells to withstand, for longer periods, the lethal effects of high cytosolic cytochrome *c*. In addition, Bcl-2 and Akt strongly suppressed microinjected cytochrome *c*-induced cell death in differentiated PC12 cells. Bcl-2 was more effective in this regard than Akt; however, their effects may simply be a reflection of levels of expression. The inhibitory effect that we observed in cytosolic extracts from PC12/Bcl2 and PC12/Akt cells correlates with a lack of procaspase 9 processing in response to cytochrome *c* addition. The specific post-mitochondrial action of AVPI-Smac/DIABLO in differentiated cells as well as up-regulation of

c-IAP-2 suggests that the caspase 9 cascade is inhibited by IAPs in differentiated cells but not in undifferentiated cells. In this regard, the induction of chicken IAP protein, ITA, by NGF in sympathetic neurons has been shown to suppress cell death in the absence of NGF (48). The AVPI motif binds to the BIR3 domain of XIAP relieving inhibition of caspase 9, which suggests that XIAP inhibition of caspase 9 is critical for cell death regulation in differentiated PC12 cells. This may explain the greater sensitivity to cytochrome *c* seen in undifferentiated cells. The observation that undifferentiated XIAP-tetracycline-repressible PC12 cells were not very sensitive to microinjected cytochrome *c* strongly indicates that XIAP-mediated inhibition of caspase 9 is acquired during a differentiation program of PC12 cells. A significant resistance to cell death induced by cytochrome *c* microinjection (greater than NGF/Bt_2cAMP-differentiated PC12 cells) has been reported in NGF-differentiated and -dependent sympathetic neurons (49). Moreover, it was shown recently that exogenous Smac/DIABLO could relieve this resistance to cytochrome *c* (50) and that deprivation of NGF results in down-regulation of XIAP (51). We have previously shown that cell death induced by deprivation of NGF/Bt_2cAMP in differentiated PC12 cells is not dependent on protein synthesis (26, 52), thus it is also likely that there are differences in the regulatory mechanisms of cell death in trophic factor-deprived differentiated PC12 cells and sympathetic neurons.

In conclusion, our PC12 data raise the possibility that during neuronal differentiation additional anti-apoptotic controls are acquired, particularly at the level of procaspase 9 processing and activation. These controls are likely to be important determinants in the long term survival of differentiated post-mitotic neurons.

Acknowledgments—We thank all the members of the Evan laboratory for their help and constructive discussions. Our thanks to Dr. Lazebnik for caspase 9 dominant negative plasmid. We are grateful to Drs. T. Littlewood, J. Downward, P. Meier, S. O'Regan, and N. Faucon Biguet for their help with the manuscript, M. Darmon for confocal microscopy, and A. Prochiantz for continued support.

REFERENCES

1. Oppenheim, R. (1991) *Annu. Rev. Neurol.* **14,** 453–501
2. Raff, M. C., Barres, B. A., Burne, J. F., Coles, H. S., Ishizaki, Y., and Jacobson, M. D. (1993) *Science* **262,** 695–700
3. Pettman, B., and Henderson, C. E. (1998) *Neuron* **20,** 633–647
4. Kuida, K., Zheng, T., Na, S., Kuan, C.-Y., Yang, D., Karasuyama, H., Rakic, P., and Flavell, R. (1996) *Nature* **384,** 368–372
5. Kuida, K., Haydar, T. F., Kuan, C.-Y., Gu, Y., Taya, C., Karasuyama, H., Su, M. S., Rakic, P., and Flavell, R. A. (1998) *Cell* **94,** 325–327
6. Motoyama, N., Wang, F., Roth, K., Sawa, H., Nakayama, K.-I., Nakayama, K., Negishi, I., Senju, S., Zhang, Q., Fujii, S., and Loh, D. (1995) *Science* **267,** 1506–1510
7. Yoshida, H., Kong, Y.-Y., Yoshida, R., Elia, A. J., Hakem, A., Hakem, R., Penninger, J. M., and Mak, T. W. (1998) *Cell* **94,** 739–750
8. De La Rosa, E., and de Pablo, F. (2000) *Trends Neurosci.* **23,** 454–458
9. Roth, K. A., Kuan, C.-Y., Hayder, T. F., D'Sa-Eipper, C., Shindler, K. S., Zheng, T. S., Kuida, K., Flavell, R. A., and Rakic, P. (2000) *Proc. Natl. Acad. Sci. U. S. A.* **97,** 466–471
10. Zaidi, A. U., D'Sa-Eipper, C., Brenner, J., Kuida, K., Zheng, T. S., Flavell, R. A., Rakic, P., and Roth, K. A. (2001) *J. Neurosci.* **21,** 169–175
11. Su, J. H., Anderson, A. J., Cummings, B. J., and Cotman, C. W. (1994) *Neuroreport* **5,** 2529–2533
12. Hartmann, A., Hunot, S., Michel, P. P., Muriel, M.-P., Vyas, S., Faucheux, B. A., Mouatt-Prignet, A., Turmel, H., Srinivasan, A., Ruberg, M., Evan, G. I., Agid, Y., and Hirsch, E. C. (2000) *Proc. Natl. Acad. Sci. U. S. A.* **97,** 2875–2880
13. Thornberry, N. A., and Lazebnik, Y. (1998) *Science* **281,** 1312–1316
14. Nicholson, D. W. (1999) *Cell Death Differ.* **6,** 1028–1042
15. Budihardjo, I., Oliver, H., Lutter, M., Luo, X., and Wang, X. (1999) *Annu. Rev. Cell Dev. Biol.* **15,** 269–290
16. Rodriguez, J., and Lazebnik, Y. (1999) *Genes Dev.* **13,** 3179–3184
17. Golstein, J. C., Waterhouse, N. J., Juin, P., Evan, G. I., and Green, D. R. (2000) *Nat. Cell Biol.* **2,** 156–162
18. Green, D. R., and Reed, J. C. (1998) *Science* **281,** 1309–1312
19. Van der Heiden, M. G., and Thompson, C. B. (1999) *Nat. Cell Biol.* **1,** E209–E216
20. Desagher, S., and Martinou, J.-C. (2000) *Trends Cell Biol.* **10,** 369–377
21. Du, C., Fang, M., Li, Y., Li, L. X., and Wang, X. (2000) *Cell* **102,** 33–42
22. Suzuki, Y., Imai, Y., Nakayama, H., Takahashi, K., Takio, K., and Takahashi, R. (2001) *Mol. Cell* **8,** 613–621
23. Martins, L. M., Iaccarino, I., Tenev, T., Gschmeissner, S., Totty, N. F., Lemoine, N. R., Savopoulos, J., Gray, C. W., Creasy, C. L., Dingwall, C., and Downward, J. (2002) *J. Biol. Chem.* **277,** 439–444
24. Datta, S. R., Brunet, A., and Greenberg, M. E. (1999) *Genes Dev.* **13,** 2905–2927
25. Kennedy, S. G., Kandel, E. S., Cross, T. K., and Hay, N. (1999) *Mol. Cell. Biol.* **19,** 5800–5810
26. Michel, P. P., Vyas, S., and Agid, Y. (1995) *Eur. J. Neurosci.* **7,** 577–586
27. Yao, R., and Cooper, G. M. (1995) *Science* **267,** 2003–2006
28. Troy, C. M., Stefanis, L., Greene, L. A., and Shelanski, M. L. (1997) *J. Neurosci.* **17,** 1911–1918
29. Troy, C. M., Rabacchi, S. A., Hohl, J. B., Angelastro, J. M., Greene, L. A., and Shelanski, M. L. (2001) *J. Neurosci.* **21,** 5007–5016
30. Deshmukh, M., Kuida, K., and Johnson, E. M., Jr. (2000) *J. Cell Biol.* **150,** 131–143
31. Srinivasula, S. M., Ahmad, M., Fernandes-Alnemri, T., and Alnemri, E. S. (1998) *Mol. Cell* **1,** 949–957
32. Juin, P., Hueber, A.-O., Littlewood, T., and Evan, G. I. (1999) *Genes Dev.* **13,** 1367–1381
33. Kluck, R. M., Bossy-Wetzel, E., Green, D. R., and Newmeyer, D. D. (1997) *Science* **275,** 1132–1136
34. Shi, Y. (2002) *Mol. Cell* **9,** 459–470
35. Fearnhead, H. O., Rodriguez, J., Govek, E.-E., Guo, W., Kobayashi, R., Hannon, G., and Lazebnik, Y. A. (1998) *Proc. Natl. Acad. Sci. U. S. A.* **95,** 13664–13669
36. Goyal, L. (2001) *Cell* **104,** 805–808
37. Liu, Z., Sun, C., Olejniczak, E. T., Meadows, R. P., Betz, S. F., Oost, T., Herrmann, J., Wu, J. C., and Fesik, S. W. (2000) *Nature* **408,** 1004–1008
38. Wu, G., Chai, J., Suber, T. L., Wu, J.-W., Du, C., Wang, X., and Shi, Y. (2000) *Nature* **408,** 1008–1012
39. Hunter, A. M., Kottachchi, D., Lewis, J., Duckett, C. S., Korneluk, R. G., and Liston, P. (2003) *J. Biol. Chem.* **278,** 7494–7499
40. Roberts, D. L., Merrison, W., MacFarlane, M., and Cohen, G. M. (2001) *J. Cell Biol.* **153,** 221–227
41. Kroemer, G., and Reed, J. C. (2000) *Nat. Med.* **6,** 513–519
42. Martinou, I., Desagher, S., Eskes, R., Antonsson, B., Andre, E., Fakan, S., and Martinou, J.-C. (1999) *J. Cell Biol.* **144,** 883–889
43. Srinivasula, S. M., Gupta, S., Datta, P., Zhang, Z., Hedge, R., Cheong, N., Fernandes-Alnemri, T., and Alnemri, E. S. (2003) *J. Biol. Chem.* **278,** 31469–31472
44. Jin, S., Kalkum, M., Overholtzer, M., Stoffel, A., Chait, B. T., and Levine, A. J. (2003) *Genes Dev.* **17,** 1–9
45. Stefanis, L., Troy, C. M., Qi, H., and Greene, L. A. (1997) *J. Neurochem.* **69,** 1425–1437
46. Li, P., Nijhawan, D., Budihardjo, I., Srinivsula, S., Ahmad, M., Alnemeri, E., and Wang, X. (1997) *Cell* **91,** 479–489
47. Saleh, A., Srinivasula, S. M., Acharya, S., Fishel, R., and Alnemri, E. S. (1999) *J. Biol. Chem.* **274,** 17941–17945
48. Wiese, S., Digby, M., Gunnersen, J., Gotz, R., Pei, G., Holtmann, B., Lowenthal, J., and Sendtner, M. (1999) *Nat. Neurosci.* **2,** 978–983
49. Deshmukh, M., and Johnson, E. M., Jr. (1998) *Neuron* **21,** 695–705
50. Deshmukh, M., Du, C., Wang, X., and Johnson, E. M., Jr. (2002) *J. Neurosci.* **22,** 8018–8027
51. Potts, P. R., Singh, S., Knezek, M., Thompson, C. B., and Deshmukh, M. (2003) *J. Cell Biol.* **163,** 789–799
52. Vyas, S., Biguet, N. F., Michel, P. P., Monaco, L., Foulkes, N. S., Evan, G. I., Sassone-Corsi, P., and Agid, Y. (2002) *Mol. Cell Neurosci.* **21,** 1–14

Human Molecular Genetics, 2004, Vol. 13, No. 19 **2183–2196**
doi:10.1093/hmg/ddh246
Advance Access published on August 4, 2004

Calcium-permeable AMPA receptors promote misfolding of mutant SOD1 protein and development of amyotrophic lateral sclerosis in a transgenic mouse model

Minako Tateno[1], Hisako Sadakata[1], Mika Tanaka[2], Shigeyoshi Itohara[2], Ryong-Moon Shin[3], Masami Miura[3], Masao Masuda[3], Toshihiko Aosaki[3], Makoto Urushitani[1], Hidemi Misawa[4] and Ryosuke Takahashi[1,*]

[1]Laboratory for Motor System Neurodegeneration and [2]Laboratory for Behavioral Genetics, Brain Science Institute, RIKEN, Wako, Saitama 351-0198, Japan, [3]Neural Circuits Dynamics Research Group, Tokyo Metropolitan Institute of Gerontology, Itabashi, Tokyo 173-0015, Japan and [4]Department of Neurology, Tokyo Metropolitan Institute for Neuroscience, Fuchu, Tokyo 183-8526, Japan

Received April 21, 2004; Revised and Accepted July 20, 2004

Mutant Cu/Zn-superoxide dismutase (SOD1) protein aggregation has been suggested as responsible for amyotrophic lateral sclerosis (ALS), although the operative mediating factors are as yet unestablished. To evaluate the contribution of motoneuronal Ca^{2+}-permeable (GluR2 subunit-lacking) α-amino-3-hydroxy-5-methyl-4-isoxazole propionic acid (AMPA)-type glutamate receptors to SOD1-related motoneuronal death, we generated *chat-GluR2* transgenic mice with significantly reduced Ca^{2+}-permeability of these receptors in spinal motoneurons. Crossbreeding of the *hSOD1*^{G93A} transgenic mouse model of ALS with *chat-GluR2* mice led to marked delay of disease onset (19.5%), mortality (14.3%) and the pathological hallmarks such as release of cytochrome *c* from mitochondria, induction of *cox2* and astrogliosis. Subcellular fractionation analysis revealed that unusual SOD1 species first accumulated in two fractions dense with neurofilaments/glial fibrillary acidic protein/nuclei and mitochondria long time before disease onset, and then concentrated into the former fraction by disease onset. All these processes for unusual SOD1 accumulation were considerably delayed by GluR2 overexpression. Ca^{2+}-influx through atypical motoneuronal AMPA receptors thus promotes a misfolding of mutant SOD1 protein and eventual death of these neurons.

INTRODUCTION

Amyotrophic lateral sclerosis (ALS) is a fatal, adult-onset neurodegenerative disease characterized by a selective loss of motoneurons in the spinal cord and brainstem (1). Mutation of Cu/Zn-superoxide dismutase (SOD1) is the most frequent cause of familial ALS (2). Introduction of such mutated SOD1 genes into mice causes ALS-like symptoms characterized by the selective death of spinal motoneurons, despite a ubiquitous expression of mutant proteins (3). Several lines of evidence have demonstrated that mutant SOD1 toxicity is not essentially due to decreased dismutase activity, but rather to a 'gain of toxic function' (4). This so-called 'oligomerization hypothesis' has recently attracted attention from ALS researchers. The hypothesis maintains that mutant SOD1 proteins are misfolded, and consequently oligomerized and aggregated, gaining toxic properties at some stage in their formation (5). The hypothesis is based on the numerous observations that SOD1-containing inclusions/high-molecular-weight-shifted protein complexes are specifically found in spinal motoneurons and their surrounding astrocytes from autopsied patients and transgenic mice carrying mutant SOD1 genes (6–8), in spinal cord extracts from mutant SOD1 transgenic mice (9–12) and in cultured motoneurons into which mutant SOD1 has been microinjected (13).

*To whom correspondence should be addressed at: Laboratory for Motor System Neurodegeneration, Brain Science Institute, Riken, 2-1 Hirosawa, Wako, Saitama 351-0198, Japan. Tel: +81 484676072; Fax: +81 484624796; Email: ryosuke@brain.riken.jp

However, in addition to this line of evidence, glutamate-induced excitotoxicity has also been implicated in the pathophysiology of ALS patients and mutant SOD1 transgenic mice (14–17). Pharmacological experiments have strongly suggested that the excitotoxicity of spinal motoneurons largely depends on Ca^{2+}-permeable α-amino-3-hydroxy-5-methyl-4-isoxazole propionic acid (AMPA) receptors specifically expressed in a subset of neurons, including spinal motoneurons (18,19). AMPA receptors, major mediators for fast excitatory neurotransmission in the mammalian central nervous system, are composed of a heteromeric complex of four subunits GluR1–GluR4, and the absence of GluR2 renders the receptor Ca^{2+}-permeable (20). As this unique property of GluR2 is generated posttranscriptionally by RNA editing, an editing failure can also produce Ca^{2+}-permeable AMPA receptors (21). Reduced editing efficiency of GluR2 mRNA has been specifically reported in spinal motoneurons from human sporadic ALS patients (22), further suggesting that Ca^{2+}-permeable AMPA receptor-mediated excitotoxicity is closely linked to the vulnerability of spinal motoneurons in ALS. However, whether and in what manner this atypical type of AMPA receptor affects mutant SOD1-induced motoneuronal degeneration remains to be elucidated.

The purpose of the present study was to explore a mechanistic link between glutamate toxicity and the conversion of mutant SOD1 into aberrant forms by modification of the electrophysiological properties of motoneuronal AMPA receptors in an ALS mouse model. The *chat-GluR2* transgenic mouse line was generated to overexpress *GluR2* in a cholinergic neuron-specific manner, resulting in a large reduction in Ca^{2+}-permeability of motoneuronal AMPA receptors. We detected various types of abnormally folded SOD1 proteins in fractions derived from different cellular compartments from *hSOD1*^{G93A} mice spinal cords. Double transgenic mice carrying both *chat-GluR2* and *hSOD1*^{G93A} displayed a marked delay of disease onset, followed by delayed formation of all the abnormal SOD1 species. These results indicate that Ca^{2+}-permeable AMPA receptors in motoneurons contribute to the conformational changes of mutant SOD1 and the subsequent neurodegeneration associated with these changes.

RESULTS

Generation and characterization of *chat-GluR2* transgenic mice: cholinergic neuron-specific GluR2 overexpression results in substantial reduction of Ca^{2+}-permeable AMPA receptors in spinal motoneurons

A mouse line with reduced numbers of Ca^{2+}-permeable AMPA receptors in spinal motoneurons was generated. Spinal motoneurons are typical cholinergic neurons, constituting a minor population among total spinal neurons. Thus, a cholinergic neuron-specific promoter, i.e. the choline acetyltransferase (*ChAT*) gene promoter (23) (Fig. 1A) was used to preferentially increase *GluR2* expression in spinal motoneurons. Three independent *chat-GluR2* transgenic lines, Tg3, Tg7 and Tg10, were established. To examine the copy number of the *chat-GluR2* transgene, Taqman quantitative DNA PCR and genomic Southern blotting were performed. Results from Taqman PCR indicated that the Tg3, Tg7 and Tg10 lines contained ~2, 10 and 16 copies of the *chat-GluR2* transgene, respectively, a finding which was also supported by genomic Southern blotting (Fig. 1B). Expression patterns of the transgenes in the spinal cord were examined using *in situ* hybridization (Fig. 1C), revealing a preferential transcription of transgenes in cholinergic neurons in *chat-GluR2* mice. To quantify the *GluR2* mRNA level in spinal motoneurons, motoneurons were carefully purified from frozen slices of spinal cord using laser microdissection, because other neuronal populations such as dorsal horn neurons express high level of *GluR2*. Quantitative PCR analysis revealed that spinal motoneurons in Tg7 expressed levels of *GluR2* mRNA nearly 5-fold higher than those of non-transgenic control mice (Table 1). Tg10 included numerous copies of the transgene, but displayed lower levels of *GluR2* expression than Tg7, probably owing to DNA methylation of transgenes (data not shown). No significant changes in mRNA levels of *ChAT*, endogenous *SOD1, GluR3* or *GluR4* were observed in *chat-GluR2* transgenic mice compared with non-transgenic mice. Western blotting of the extracts prepared from the spinal cord ventral region also revealed a significant increase of the GluR2 protein level in Tg7 compared with that in non-transgenic littermates (Fig. 1D). *GluR2* expression was thus significantly increased in spinal motoneurons in *chat-GluR2* mice without affecting the expression of other AMPA receptor subunits. Next, the Ca^{2+}-permeability of AMPA receptors in spinal motoneurons was examined. Whole-cell patch-clamp recordings were performed on motoneurons in spinal cord slices. The first two graphs in Figure 1E represent typical I-V relationships, showing distinct inward rectification in wild-type (wt), whereas a linear relationship is seen in Tg7. Normalized I–V relationships reveal a clear difference between wt and Tg7 ($P < 0.001$). The rectification index, an index of Ca^{2+}-permeability calculated as the ratio of chord conductance at +40 and −70 mV, was estimated as 0.262 ± 0.024 for wt and 0.436 ± 0.038 for Tg7 (mean ± SEM, $P < 0.001$). Thus, the majority of AMPA receptors in spinal motoneurons were Ca^{2+}-impermeable in Tg7 mice, but were Ca^{2+}-permeable in non-transgenic controls.

Crossbreeding *hSOD1*^{G93A} transgenic mice with *chat-GluR2* transgenic mice markedly delays disease onset and mortality

The *chat-GluR2* transgenic mouse was mated with a *hSOD1*^{G93A} transgenic ALS mouse to generate double transgenic (GS) mice. Most of the spinal motoneuronal AMPA receptors were actually Ca^{2+}-impermeable in GS mice, but Ca^{2+}-permeable in littermates carrying only the *hSOD1*^{G93A} transgene (*S* mice, Fig. 2A). The G1L line of *hSOD1*^{G93A} mice develops overt symptoms defined as disease onset at around 7 months, a classification based on a sudden decrease in motor performance in behavioral tests such as the rotarod test (25,26). Death occurs at around 8.5–9 months. To evaluate the effects of reduced Ca^{2+}-permeability in AMPA receptors on the clinical course of ALS, motor performance was assessed by the rotarod test. Figure 2B depicts the rotarod score of each mouse measured every week, clearly showing that mice carrying the *SOD1*^{G93A} gene are rapidly declining

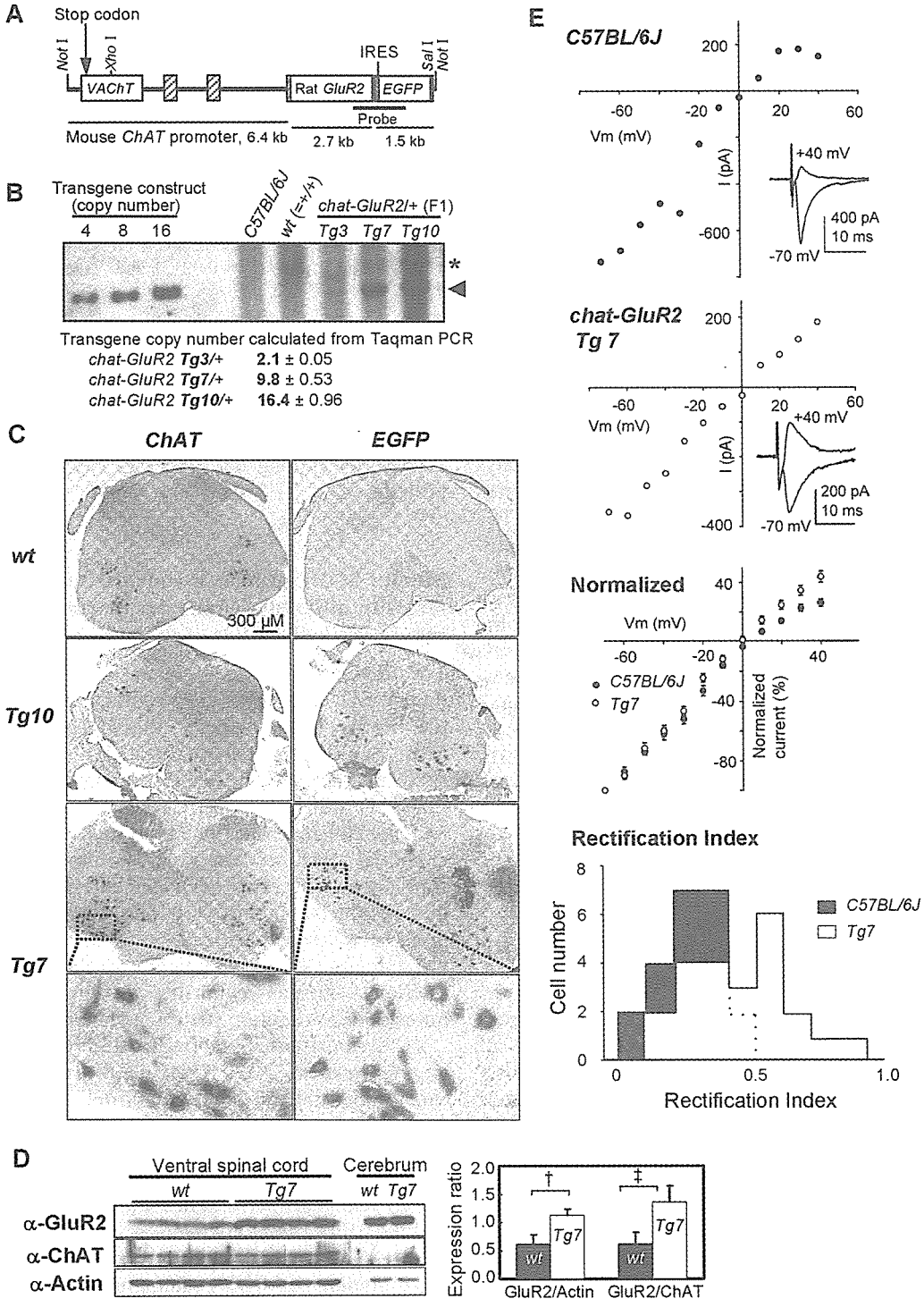

Figure 1. Generation and characterization of *chat-GluR2* transgenic mice. (**A**) The DNA fragment introduced into *chat-GluR2* transgenic mice contains the rat *GluR2* and *EGFP* coding sequences driven by mouse *ChAT* promoter. *GluR2* and *EGFP* are transcribed into the same mRNA, but are independently translated owing to the IRES. The striped and filled boxes represent exons of the endogenous *ChAT* gene and SV40 polyadenylation signal, respectively. (**B**) Transgene copy number was examined by genomic Southern blotting using the probe indicated in (A) (24) and by Taqman quantitative DNA PCR. The arrowhead indicates the *Xho* I–*Sal* I-digested 9.0 kb fragment of the transgene. (**C**) Transgene expression is predominant in cholinergic neurons. Either digoxigenin-labeled *EGFP* or *ChAT* riboprobe was used to hybridize to spinal cord sections. Both *EGFP* and *ChAT* were preferentially expressed in large cells (diameter $\geq$25 μm) located in the ventral horn, representing spinal motoneurons. (**D**) The GluR2 protein level is increased in the ventral half of the spinal cord in *chat-GluR2* transgenic mice. The ventral half was carefully dissected from T10–L5 segments of spinal cords. Extracts of ventral spinal cords (40 μg, $n = 4$) and cerebrum (10 μg, $n = 2$) were immunoblotted. † $P < 0.05$, ‡ $P < 0.01$. (**E**) The majority of AMPA receptors in spinal motoneurons were Ca^{2+}-impermeable in *chat-GluR2* transgenic mice. The excitatory postsynaptic potential (EPSC) of AMPA components was measured from 23 motoneurons of *chat-GluR2* transgenic mice (Tg7, $n = 11$) and 22 motoneurons of non-transgenic C57BL/6J mice (wt, $n = 9$), using the whole-cell patch-clamp method. Insets represent synaptic currents at holding potentials of −70 and +40 mV.

Table 1. GluR2 mRNA level is to increased in motoneurons of *chat-GluR2* transgenic mice

Mouse	GluR2	GluR3	GluR4	ChAT	SOD1
C57BL/6J ($n = 3$)	1.00	1.00	1.00	1.00	1.00
GluR2-Tg3 ($n = 3$)	0.96 ± 0.27	0.91 ± 0.13	1.23 ± 0.27	1.01 ± 0.16	0.74 ± 0.20
GluR2-Tg7 ($n = 3$)	4.78 ± 0.85*	1.02 ± 0.54	1.21 ± 0.26	1.17 ± 0.38	1.09 ± 0.41
GluR2-Tg10 ($n = 6$)	1.58 ± 0.38**	0.92 ± 0.92	1.22 ± 0.48	1.15 ± 0.58	1.02 ± 0.15

Motoneurons in spinal cord were collected using laser microdissection. Transcription levels of several genes were examined by Taqman real-time quantitative PCR. Data were normalized with *GAPDH* expression and then represent relative expression levels compared with levels in C57BL/6J non-transgenic control mice (mean ± SD). Not significantly different ($P > 0.05$) except for *($P = 0.0015$) and **($P = 0.0184$), compared with non-transgenic controls.

in performance score after a certain period. The day just before the decline in score was defined as the day of disease onset, and the mean time of disease onset was compared between S and GS littermates. Disease onset in GS mice was delayed, by 42.9 days (19.5%) in Tg7 and 18.7 days (8.5%) in Tg10, as compared with S mice. Lifespan was also prolonged in GS mice, by 37.5 days (14.3%) in Tg7 and 15.2 days (5.7%) in Tg10 (Fig. 2C, Table 2). No significant difference in rotarod score or lifespan was observed between the *chat-GluR2* and wt mice (data not shown). Furthermore, no prolongation of lifespan was observed in the GS mice generated from Tg3 (data not shown), which animals displayed no additional *GluR2* expression in spinal motoneurons (Table 1). The number of motoneurons in the spinal cord was counted, revealing that degeneration of motoneurons was also delayed in GS mice from the Tg7 line (Fig. 2D). All these results indicate that reducing Ca^{2+}-permeability in AMPA receptors delays disease onset and motoneuron death caused by mutant SOD1, presumably in a dose-dependent manner.

cytochrome *c*-release from mitochondria, *cox2*-induction and gliosis are delayed by GluR2 overexpression

We next investigated whether pathological changes related to disease onset are verifiably affected by overexpression of GluR2. Of the numerous events accompanying disease onset in $hSOD1^{G93A}$ mice, we focused on cytochrome *c*-release from mitochondria and induction of cyclooxygenase-2 (*cox-2*), as a treatment of $hSOD1^{G93A}$ mice with agents inhibiting these events delays disease onset (26,27). Cytochrome *c*, which is normally localized to the intermembrane space of mitochondria, activates caspases and subsequent apoptosis after release into the cytosol (28). Cox-2 catalyzes the synthesis of prostaglandin E2, which stimulates glutamate release from astrocytes and plays a key role in the inflammatory process (29). Cytosolic extracts (26) and RNA were prepared from the spinal cord lumbar region, as this is the most severely affected region in ALS. Cytochrome *c* became clearly detectable in the cytosolic fraction around 7 months in S, but was only faintly detectable even at 8 months in GS littermates, indicating that the release of cytochrome *c* is considerably delayed in *GS* mice (Fig. 3A). Induction of *cox-2* transcription was also significantly delayed in GS in comparison to S littermates (Fig. 3B). After disease onset, $hSOD1^{G93A}$ mice exhibit severe gliosis in the spinal cord owing to exacerbated inflammation (30). We also found that astrogliosis was remarkably delayed in GS mice (Fig. 3C). Reducing Ca^{2+}-permeability of AMPA receptors is thus likely to affect the upstream events of cytochrome *c*-release and *cox-2* induction among the processes triggered by mutant SOD1 proteins.

Mutant SOD1 protein is converted into various unusual forms in different cellular compartments, but the conversion is markedly delayed by GluR2 overexpression

The misfolding and subsequent conformational changes in mutant SOD1 proteins are hypothesized to be responsible for the death of motoneurons in SOD1-related ALS (5,9,10). Most SOD1 proteins are located in the cytosol, but very small populations are found in organelles such as mitochondria (31) and nuclei (32). Therefore, we roughly divided a homogenate from the lumbar spinal cord into a crude mitochondrial fraction and a post-mitochondrial fraction by simple centrifugation (31), and analyzed in which fraction the misfolded and hence high-molecular-weight-shifted SOD1 proteins were detectable. Most organelles and cytoskeletons were found to be contained in the crude mitochondrial fraction, whereas cytosolic proteins were in the post-mitochondrial fraction (data not shown).

As the post-mitochondrial fraction contained an extremely large amount of SOD1 proteins, it was a formidable task to detect high-molecular-weight-shifted SOD1 species in this fraction by conventional western blotting (data not shown). To enhance the sensitivity of detection, the post-mitochondrial fraction was size-fractionated using size-exclusive chromatography with high-performance liquid chromatography (HPLC), and the HPLC fractions were immunoblotted. The results as shown in Figure 4A indicated that, in addition to the very large amount of SOD1 monomers, high-molecular-weight-shifted SOD1-immunopositive species corresponding to dimer (*2), trimer (*3) and tetramer (*4) sizes of mutant SOD1 were detectable in 2-, 6- and 8-month-old S mice, respectively (Fig. 4A). These oligomer-sized species were not observably detected in the lumbar spinal cord from wt or the cerebrum from S littermates even at 8 months, suggesting that the conversion of the SOD1 protein into oligomer-sized forms preferentially occurs in the spinal cord. The molecular shifts of those species were not due to ubiquitination, as they were not detected by anti-ubiquitin antibody (Supplementary Material, Fig. S1). Formation of oligomer-sized SOD1 aberrant forms

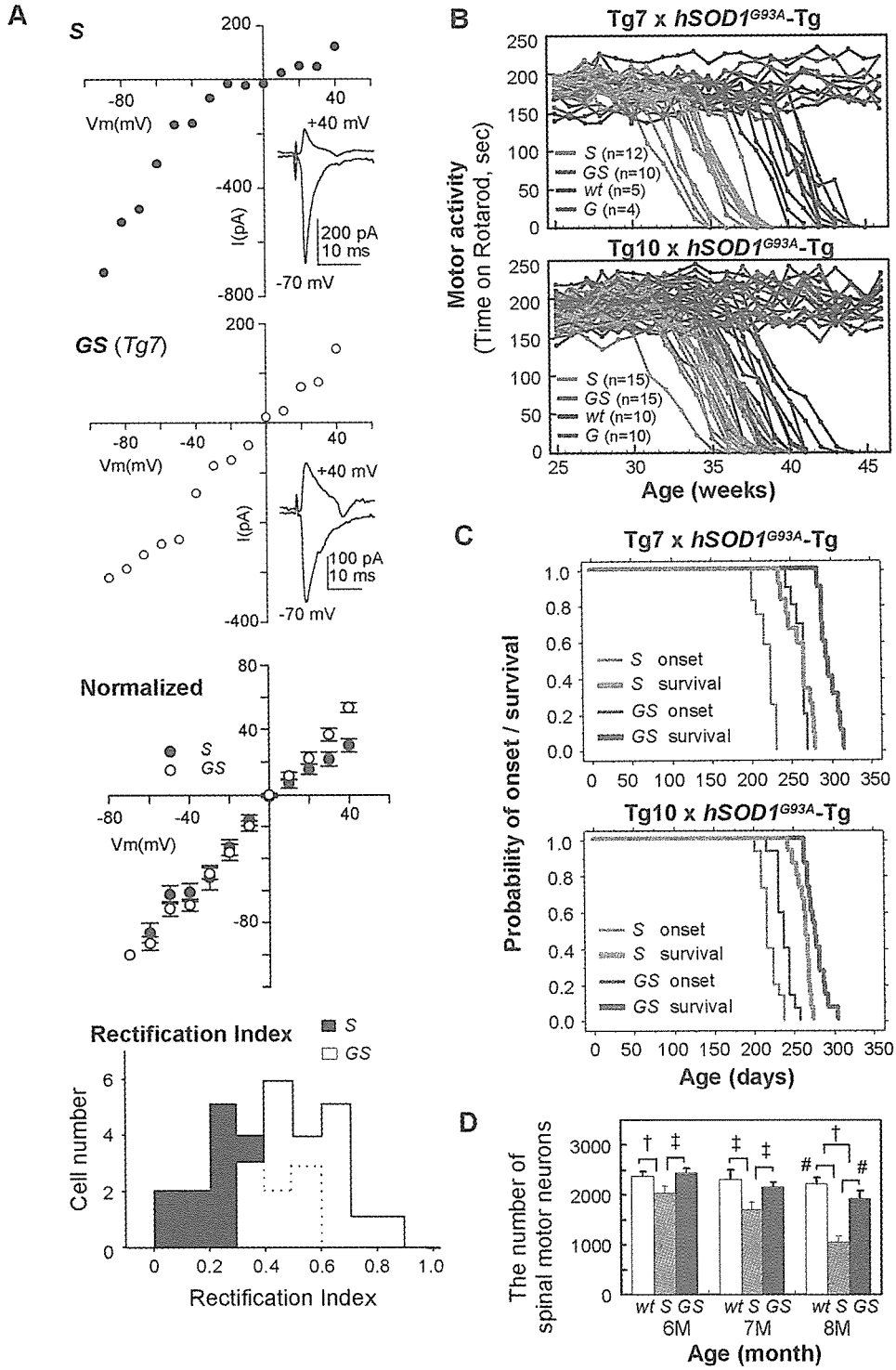

Figure 2. GluR2 overexpression markedly delays disease onset and prolongs survival in *hSOD1*^{G93A} transgenic mice. (**A**) The majority of AMPA receptors in spinal motoneurons were Ca^{2+}-impermeable in GS (*chat-GluR2/+;hSOD1*^{G93A}/+) littermates, but Ca^{2+}-permeable in S (*hSOD1*^{G93A}/+) littermates. EPSCs of AMPA components were measured from 19 (S, $n = 5$) and 21 (GS, $n = 4$) spinal motoneurons in the same way as in Figure 1E. Rectification index was estimated as 0.321 ± 0.036 for S and 0.535 ± 0.018 for GS (mean ± SEM, $P < 0.01$). (**B**) GluR2 overexpression delayed the decline of motor performance assessed by the rotarod test. Each point represents the mean of four measurements per day every week on each mouse. Significance of difference in comparison of GS versus S littermates was analyzed by repeated measured ANOVA followed by Fisher's PLSD *post hoc* test (Tg7: $P < 0.0001$ and Tg10: $P = 0.0005$). In both lines, $P < 0.001$ after 32 weeks of age. (**C**) Cumulative probability of disease onset and survival was compared between S and GS littermates. Data were analyzed by Kaplan-Meier life test and log-rank test, and the result is summarized in Table 2. (**D**) Degeneration of spinal motoneurons was significantly delayed by GluR2 overexpression. The 30 μm thick frozen sections were prepared from T10–L5 segments of spinal cords and stained with 0.01% toluidine blue. Large neurons with diameter >25 μm in the ventral horn, which are most severely depleted in *hSOD1*^{G93A} mice, were counted serially in all sections. Data represent the means ± SEM from 4–6 mice in each stage. † $P < 0.05$, ‡ $P < 0.01$ and # $P < 0.001$.

Table 2. Prolonging effects of *GluR2* overexpression on the disease onset and survival

chat-GluR2-Tg		*hSOD1*^{G93A}/+	*chat-GluR2*/+, *hSOD1*^{G93A}/+	*P*
Tg7	Onset	219.7 ± 3.0	262.6 ± 2.6	<0.0001
	Survival	262.5 ± 4.5	300.0 ± 3.5	<0.0001
	Length	42.8 ± 2.2	37.9 ± 2.4	0.1563
	n	12	10	
Tg10	Onset	219.8 ± 2.6	238.5 ± 2.7	<0.0001
	Survival	264.5 ± 2.2	279.7 ± 3.1	0.0005
	Length	44.8 ± 2.0	40.8 ± 2.0	0.2189
	n	15	15	

Data are expressed as means ±SEM. Statistical significance in comparison of *hSOD1*/+ (S) and *chat-GluR2*/+ *hSOD1*/+ (GS) littermates was assessed by ANOVA followed by *post hoc* Fisher's PLSD test.

was significantly delayed in GS compared with S littermates. On the other hand, western blotting of the crude mitochondrial fractions revealed that a significant population of SOD1 proteins in this fraction was converted into species distinct from those found in the post-mitochondrial fractions (Fig. 4B). In addition to dimer-sized SOD1, two major species between the monomer and dimer sizes (~25 and 35 kDa) were detected in symptomatic mice. Formation of all the unusual species in crude mitochondrial fractions was also delayed by more than 1 month in GS compared with S littermates.

Certain populations of SOD1 proteins, probably growing aggregates, can be efficiently trapped onto membranes composed of cellulose acetate, and these filter-trapped SOD1 species extensively increased in tandem with disease progression in mutant SOD1 transgenic mice (10). Figure 4C indicates that the filter-trapped SOD1 aggregates were considerably increased during disease onset in S mice, but increased more slowly in GS compared with S littermates.

Unusual SOD1 species first accumulate in the fractions dense with neurofilaments, GFAP, nuclei and mitochondria, which accumulation is markedly delayed by GluR2 overxpression

The finding of unusual SOD1 species depicted in Figure 4 led us to do further subcellular fractionation analysis in order to define in which cellular component such unusual species are localized. We thus divided the lumbar spinal cord into four different organelle-enriched fractions (P1–P4) and a supernatant fraction (S) consisting of cytosolic proteins (Fig. 5A). Immunoblots of these fractions revealed that unusual SOD1 species (*) first appeared in the P1 and P2 fractions long time before disease onset, and then, intensively accumulated into the P1 fraction by the disease onset (Fig. 5B). Nuclei and certain kinds of cytoskeletons such as neurofilaments and glial fibrillary acidic protein (GFAP) were effectively concentrated into the P1 fraction, whereas mitochondria are concentrated into the P2 fraction. In S mice, the dimer-sized species were first detected in the P1 and P2 fractions at 4 months. At 7 months, the stage of disease onset, the P1 fraction contained a considerable amount of unusual SOD1 species of approximately the size of a dimer, 25 and 35 kDa, which were very similar to those detected in the crude mitochondrial fractions as depicted in Figure 4B. These species were only weakly detected in P2, P3 and P4 fractions at the stage of disease onset, but then accumulated with disease progression. All these unusual SOD1 species were hardly detectable in the cerebrum, cerebellum, testis and muscle from S mice even at end stage (data not shown for cerebellum and muscle), and were hardly detectable in the spinal cord from 9-month-old wt littermates. In GS littermates, dimer-sized species were faintly detected in the P1 and P2 fractions at 6 months of age. Other species accumulated to an enormous extent in the P1 fraction at 8 months of age, the stage of disease onset in GS mice, indicating that the formation of these unusual SOD1 species was delayed concomitantly with the delay of disease onset in GS compared with S littermates. These observations strongly suggest that the misfolding and subsequent conformational changes of mutant SOD1 proteins are delayed when the Ca^{2+}-permeability of AMPA receptors is significantly reduced.

The increase of oxidatively modified proteins is attenuated by GluR2 overexpression

Although the mechanism underlying the marked effects of reduced AMPA receptor Ca^{2+}-permeability on the conformational changes of mutant SOD1 is currently unclear, the attenuation of cellular oxidative stress may be involved. Oxidation of human SOD1 proteins *in vitro* causes cleavage and/or conjugation (33), resulting in the formation of various types of unusual SOD1 species (34,35). Moreover, elevated cellular oxidative stress and resulting oxidative modification of proteins and lipids such as carbonylation are reported in spinal cords from *hSOD1*^{G93A} mice (36–38). Thus, we compared the level of carbonylated proteins in spinal cord extracts between S and GS littermates, taking it as a marker of cellular oxidative stress. The results in Figure 6 reveal that carbonylated proteins in spinal cords increased only gradually before disease onset, then, increased substantially at disease onset in both S and GS mice. Such drastic increase was not observed in the extracts from cerebrum even in 9-month-old S mice. Statistical analysis revealed that the increase of carbonylation was significantly delayed, by at least 2 months, in GS compared with S littermates. This delay of protein oxidative modification might help explain why conformational changes of SOD1 proteins are delayed in GS mice.

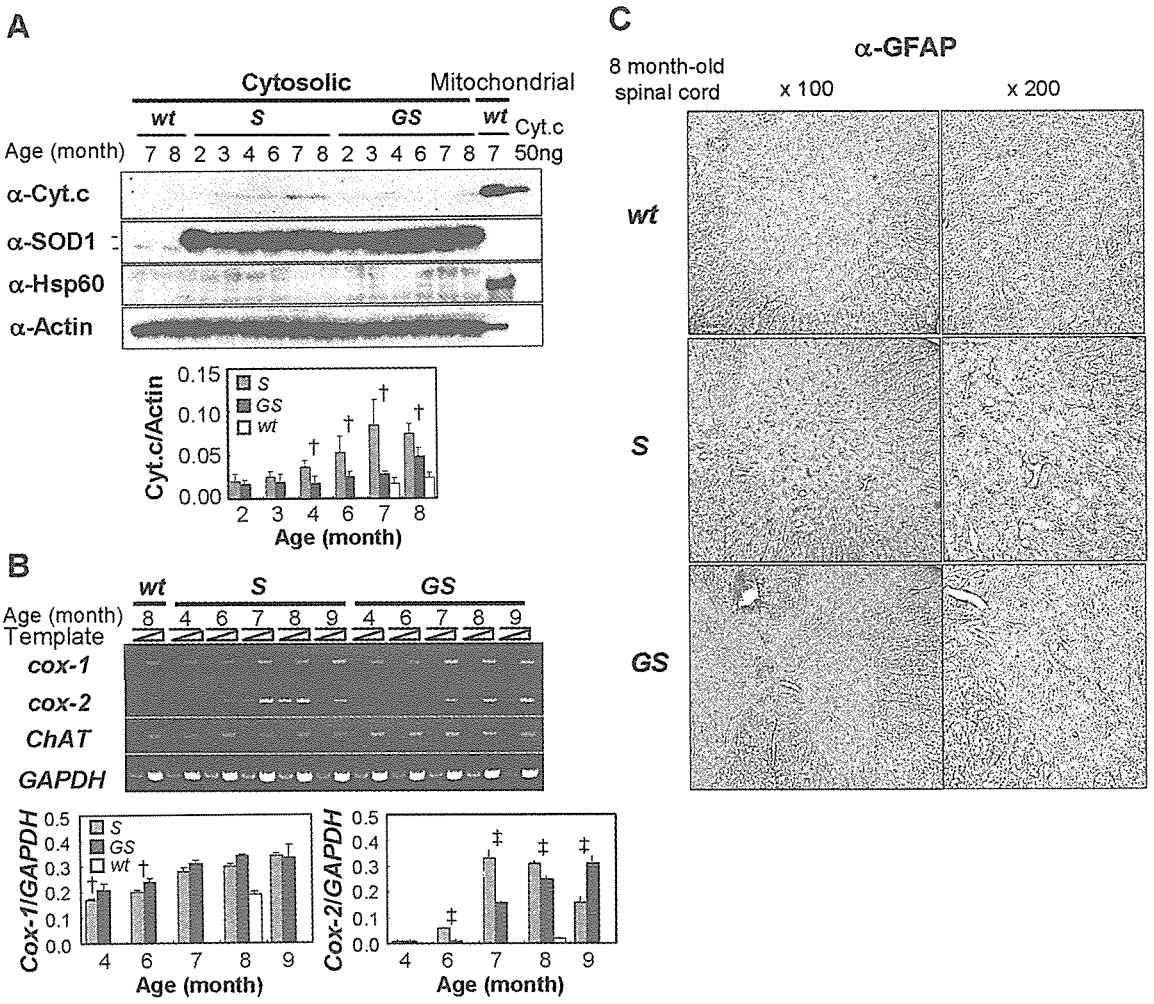

Figure 3. GluR2 overexpression delays cytochrome *c*-release from mitochondria, *cox-2* induction and subsequent astrogliosis. (**A**) Cytochrome *c* release from mitochondria into the cytosol was markedly delayed by GluR2 overexpression. Cytosolic (15 μg) and crude mitochondrial (2 μg) fractions from the lumbar spinal cords were immunoblotted. Hsp60 was used as a marker protein for mitochondria. The anti-SOD1 antibody used in this paper recognizes both human (upper band, 22 kDa) and mouse (lower band, 16 kDa) SOD1. † $P < 0.05$, in comparison of S and GS littermates. (**B**) Induction of *cox-2* transcription was significantly delayed by GluR2 overexpression. RT–PCR analysis was performed using total RNA extracted from lumbar spinal cords. To confirm exponential amplification in each PCR condition, results using two dilution series of template, which differed in concentration by an order of magnitude, are shown. Significance of difference was assessed from the results using larger amounts of templates. † $P < 0.05$ and ‡ $P < 0.01$ (S versus GS). (**C**) Astrogliosis was prominent in 8-month-old S, but was barely detected in GS littermates at the same age. The lumbar regions of mouse spinal cords were immunostained with anti-GFAP antibody.

DISCUSSION

Motoneuronal Ca^{2+}-permeable AMPA receptors contribute to selective cell death in SOD1-related ALS

The present study demonstrates that motoneuronal Ca^{2+}-permeable AMPA receptors contribute to the development of SOD1-related ALS. Reducing permeability by motoneuron-preferential GluR2 overexpression significantly prolongs the lifespan of ALS mice by delaying disease onset (Fig. 2B and C). The mutant SOD1 protein level in the ventral spinal cord was not significantly different between S and GS littermates (Supplementary Material, Fig. S2), and *GluR2* mRNA level in spinal motoneurons did not significantly change during the course of disease in *hSOD1*^{G93A} mice (data not shown). Thus, the beneficial effects of GluR2 overexpression do not result from either a reduction of mutant SOD1 expression or a simple compensation of decreased GluR2 expression, but from reduced Ca^{2+}-influx through motoneuronal AMPA receptors.

A recent study on chimeric mice between wild-type and mutant SOD1 transgenic mice revealed that the death of motoneurons expressing mutant SOD1 can be delayed when the surrounding non-neuronal cells do not express mutant SOD1 (39). This finding indicates that motoneuronal death triggered by mutant SOD1 is not cell-autonomous, but also depends on the interactions with surrounding glial cells expressing mutant SOD1. However, there must be a reason why only motoneurons die among the neurons surrounded by non-neuronal cells expressing mutant SOD1. The present study provides evidence that the expression of Ca^{2+}-permeable AMPA receptors confers a critical feature on motoneurons such that they undergo death in response to mutant SOD1 effects within themselves and surrounding cells.

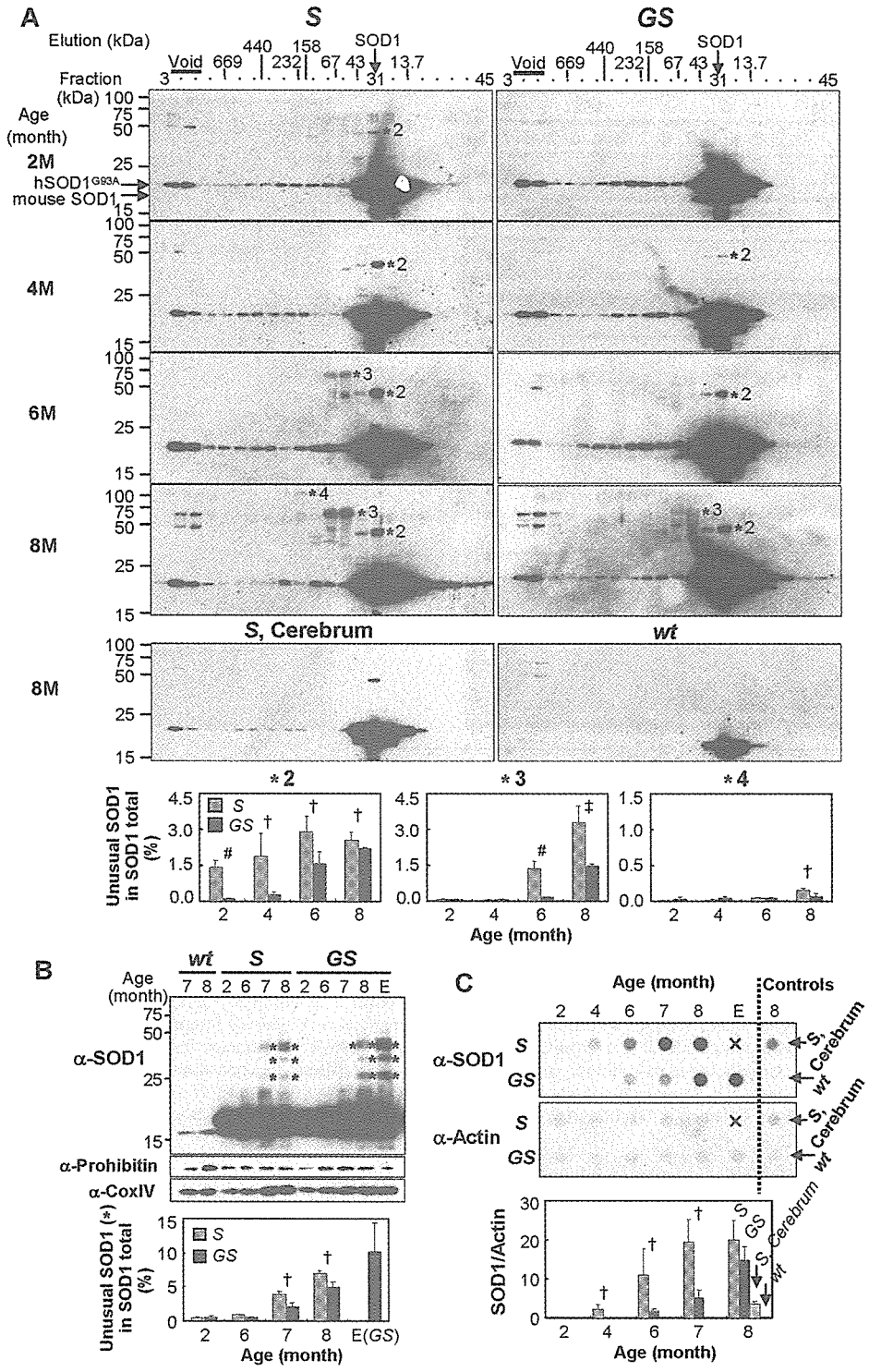

Figure 4. Distinctive patterns of unusual SOD1 species are found in the fractions derived from the cytosol and organelle/cytoskeleton, the formation of which is markedly delayed by GluR2 overexpression. (**A**) A very small population of SOD1 proteins is converted into oligomer-sized species in the cytosol long before disease onset, which was effectively delayed by GluR2 overexpression. HPLC fractions derived from ~100 μg of post-mitochondrial (cytosolic protein-enriched) fractions were immunoblotted. Formation of unusual SOD1 species corresponding to a dimer (*2), a trimer (*3) and a tetramer (*4) in size was significantly delayed in GS compared with S littermates. † $P < 0.05$, ‡ $P < 0.01$ and # $P < 0.001$. Non-specific bands appear in the void fraction. (**B**) Unusual SOD1 species differing from those in post-mitochondrial fractions were detected in crude mitochondrial (organelle/cytoskeleton-enriched) fractions at disease onset, which was effectively delayed by GluR2 overexpression. The crude mitochondrial fractions (5 μg) were immunoblotted. Asterisks indicate usual SOD1 species corresponding to a dimer, ~25 and 35 kDa sizes. † $P < 0.05$ (S versus GS littermates). (**C**) Filter-trapped SOD1, which might represent misfolded or aggregated forms, increased markedly before disease onset in S, but very slowly in GS littermates. Aliquots 12.5 μg of the post-mitochondrial fractions were solubilized with TBST (0.025% Tween-20) and filtered using cellulose acetate membrane (0.2 μm diameter) followed by immunostaining (10). † $P < 0.05$ (S versus GS littermates).

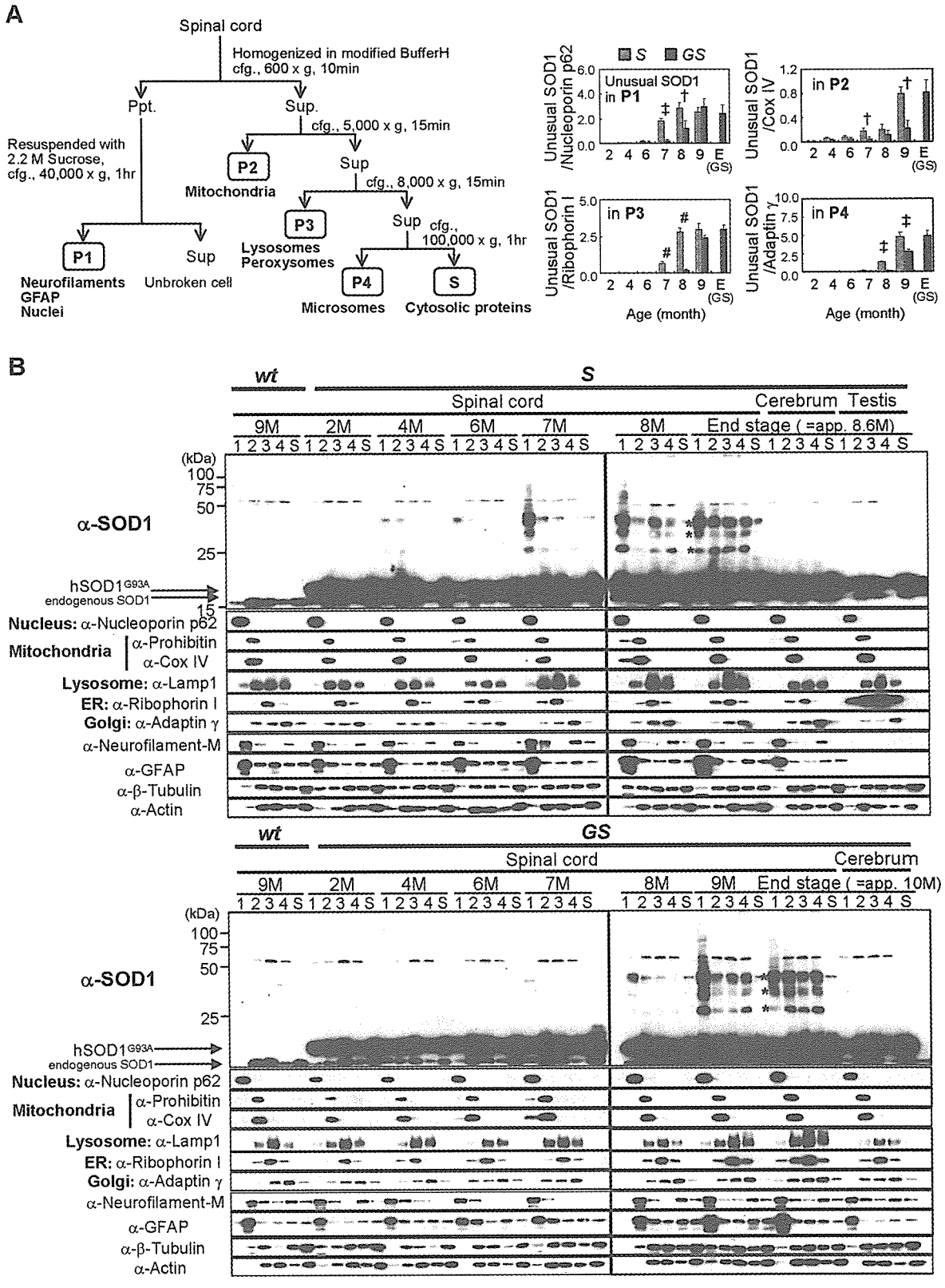

Figure 5. Unusual SOD1 species first appear in the fraction enriched in neurofilaments, GFAP, nuclei and mitochondria, which is markedly delayed by GluR2 overexpression. (**A**) The procedure for subcellular fractionation. The representative organelles and cytoskeletons enriched in each fraction are indicated. (**B**) Unusual SOD1 species (asterisks) were first detected in P1 and P2 before disease onset, and then accumulated in other organelle fractions with disease progression. Aliquots of 5 μg of each fraction was immunoblotted. The distribution of each organelle and cytoskeletons was evaluated using antibodies for each marker protein. Accumulation of unusual SOD1 species in spinal cords was significantly delayed in GS compared with S littermates. † $P < 0.05$, ‡ $P < 0.01$ and # $P < 0.001$ (S versus GS littermates).

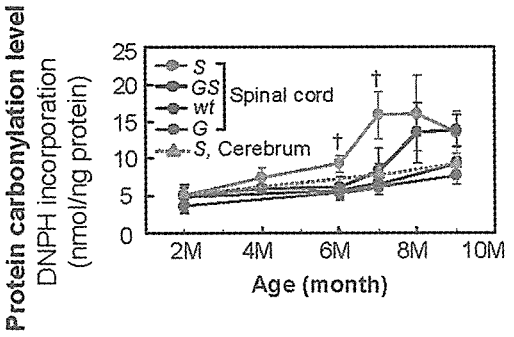

Figure 6. Oxidative modification of proteins is slowly increased by GluR2 overexpression. Tissue extracts were treated with DNPH, which specifically reacted with carbonyl groups in the protein side chains and converted into DNP–hydrazone. The levels of carbonylated proteins in spinal cords, which were evaluated from the absorption of DNP–hydrazone (375 nm), were significantly higher in the 6- and 7-month-old S littermates and 8-month-old GS littermates compared with G and wt littermates ($P < 0.05$). In comparison between the S and GS littermates, the carbonylated protein levels were significantly higher in S than GS littermates at the age of 6 and 7 months († $P < 0.05$). $n = 3–4$ mice per each group.

Ca^{2+}-influx though motoneuronal AMPA receptors promotes conversion of SOD1 protein into aberrant forms

In addition to delaying the disease onset, GluR2 overexpression succeeded in delaying the conversion of SOD1 protein into unusual forms (Figs 4 and 5B). To date, more than 20 papers have reported the delay of disease onset in mutant SOD1 transgenic mice by various pharmacological or transgenic techniques (1). However, the effects of such trials on SOD1 conformational changes have yet to be shown. Here, we provide the first evidence that disease onset is delayed when conversion of SOD1 into unusual forms is delayed, consistent with the hypothesis that SOD1 aggregation participates in ALS pathogenesis.

This study also provides an outline of the temporal profile for the formation of unusual SOD1 species during the clinical course of mouse ALS. Previous studies with western blots detected two distinct patterns of unusual SOD1 species in spinal cord extracts from mutant SOD1 transgenic mice. One is a set of oligomer-sized species (9), and another contains species between a monomer and dimer in size (10–12). Here, we show that trimer- and tetramer-sized species are detectable in the post-mitochondrial fractions containing cytosolic proteins (Fig. 4A), whereas species between a monomer and dimer in size are detected in the crude mitochondrial fractions containing major cellular components such as organelles and cytoskeleton. On the other hand, dimer-sized species were detectable in both fractions (Figs 4B and 5B). The amount of trimer and tetramer-sized species in the cytosol seemed comparatively very small to the unusual species in the organelle/cytoskeleton fractions, as these species are no longer detectable in Figure 5B, an experiment in which the same subcellular fraction amounts were loaded to the respective lanes. The first detectable unusual SOD1 species are dimer-sized species that appear several months before disease onset. Subsequently, a very small population of SOD1 proteins grows into trimer- and tetramer-sized species in the cytosol. On the other hand, a large amount of SOD1 protein is converted into ~25 and 35 kDa-sized species. These unusual species first appear in the P1 and P2 fractions and then extensively accumulate into the P1 fraction by disease onset. The presence in the P2 mitochondrial fraction might be related to the dysfunction of mitochondria that has been reported in *hSOD1*^{G93A} mice around disease onset (1,31). In the P1 fraction, nuclei and certain kind of filamentous cytoskeletons such as neurofilaments and GFAP, but not actin filaments or microtubiles, are effectively concentrated. The extensive accumulation of unusual SOD1 species in the P1 fraction implies that these species are fundamentally associated with neurofilaments or GFAP, because a further fractionation study revealed that these species do not independently accumulate in the nuclei (data not shown). Abnormalities in the neurofilaments observed in ALS patients and mutant SOD1 mice, such as an accumulation of neurofilament inclusions (1) and a defect in axonal transport (4), might be closely related to this phenomenon. Alternatively, those SOD1 species might be involved in aggresome-like structures, as observed in HEK293 cells transfected with G85R and G93A SOD1 mutants (9). After disease onset, unusual species spread to other organelle fractions enriched in lysosomes, peroxysomes and microsomes derived from the endoplasmic reticulum (ER), Golgi apparatus and plasma membrane. These alterations in SOD1 proteins are thought to predominantly occur in motoneurons and surrounding astrocytes, as SOD1-containing proteinacious inclusions, which are likely to have developed from high-molecular-weight-shifted SOD1 species, are specifically detected in motoneurons and neighboring astrocytes in end-stage *hSOD1*^{G93A} mice (6–8). The reduction of Ca^{2+}-influx through motoneuronal AMPA receptors successfully delayed the formation of the entire range of unusual SOD1 species in the spinal cord extracts (Figs 4 and 5A) as well as the development of astrogliosis (Fig. 3C). These results suggest that Ca^{2+}-influx through motoneuronal AMPA receptors can affect the physiology of neighboring astrocytes as well as their own, and contributes to the misfolding and subsequent conversion of SOD1 protein.

Ca^{2+}-influx through AMPA receptors enhances ROS production, which may induce the misfolding of SOD1 proteins

Ca^{2+}-influx through motoneuronal AMPA receptors seems to enhance oxidative stress primarily in motoneurons and secondarily in neighboring astrocytes. Activation of Ca^{2+}-permeable AMPA receptors causes rapid increases in the level of cytosolic calcium, which are rapidly attenuated by trapping with Ca^{2+}-chelating proteins and by incorporation of calcium into mitochondria and ER (40). As spinal motoneurons are less capable of buffering increased calcium levels, probably due to a lack of major Ca^{2+}-chelating proteins such as parvalbumin and calbindin D28K (41), a large proportion of free calcium is reported to be incorporated into mitochondria, resulting in enhanced ROS production (42). Evidence suggests that ROS generated in motoneurons can exit from the motoneurons and cause oxidative disruption of glutamate transporters and increased ROS level in neighboring

astrocytes (43). The loss of astrocytic glutamate transporters, which has been preferentially observed in the affected area in ALS patients and mouse models (15,43,44), accelerates AMPA receptor-mediated Ca^{2+}-influx and ROS generation within motoneurons, resulting in a vicious cycle to enhance the oxidative stress in motoneurons and neighboring astrocytes (45).

Enhanced ROS levels might, in part, account for the formation of unusual SOD1 species, as oxidative modification by ROS has been shown to convert SOD1 proteins into a variety of unusual forms, at least *in vitro* (34,35). We found a good correlation between the levels of carbonylated proteins and unusual SOD1 species in the spinal cord extracts from S and GS mice. Both levels were rapidly increased at disease onset, but these increases were similarly attenuated when the Ca^{2+}-permeability of AMPA receptors was reduced (Figs 4, 5B and 6). This correlation may imply that the increased cellular oxidative stress resulting from activation of motoneuronal Ca^{2+}-permeable AMPA receptors induces the misfolding and subsequent conversion of SOD1 protein within motoneurons and adjacent glial cells.

MATERIALS AND METHODS

The sequence information for the primers and probes is described in Supplementary Material, Table S1. All the data shown are representative of three mice per group when the number of mice (n) used for experiments is not mentioned. Signals in immunoblots and RT–PCR were quantified with NIH image software (1.61J). Statistical significance was assessed by the two-tailed Student's t-test when the statistical method is not mentioned. All protein electrophoreses in this paper utilized SDS–PAGE under reducing conditions. Antibodies were used for immunoblots and immunohistochemistry, which comprised of: anti-SOD1 (Stressgen, SOD-100), anti-GluR2 (BD PharMingen, 556341), anti-ChAT (Chemicon, AB144P), anti-cytochrome *c* (BD PharMingen, 556433), anti-Hsp60 (Sigma, H4149), anti-actin (Chemicon, MAB1501), anti-GFAP (Chemicon, MsX GFAP), anti-prohibitin (NeoMarkers, MS-261-P0), anti-CoxIV (Molecular Probes, A-6431), anti-nucleoporin p62 (BD Transduction Laboratories, N43620), anti-ribophorin I (Santa Cruz, sc-12164), anti-Lamp1 (BD PharMingen, 553792), anti-adaptin gamma (BD Transduction Laboratories, A36120), anti-neurofilament-M (Chemicon, AB1987), and anti-beta-tubulin (Sigma, T 4026) antibodies.

Generation of GluR2 transgenic mice

The transgene construct contained the 6.4 kb promoter region of the mouse *ChAT* gene (AF019045), the 2.6 kb rat *GluR2* coding sequence (CDS, M85035), internal ribosome entry sequence (IRES), *EGFP* CDS and the SV40 polyadenylation signal, in that order. As the *ChAT* promoter region contains an open reading frame of a vesicular acetylcholine transporter (*VAChT*) intronless gene (23), we introduced a stop codon at the 55th amino acid position to avoid producing a functional VAChT protein from this construct. The region from *IRES* to the polyadenylation signal was derived from the pIRES2–EGFP vector (Clonetech), with a base substitution so as to delete a *Not*I site in the *EGFP* 3′-untranslated region. The *Not*I-digested 10.9 kb DNA fragment was injected into C57BL/6J mouse eggs, and three transgenic lines, Tg3, Tg7 and Tg10, were established.

Taqman quantitative DNA PCR was performed using probe–primer sets specific to *EGFP* and two internal control genes, *SOD1* and *CPTI*, on an ABI7700 thermal cycler (PE Biosystems) under the conditions recommended by the manufacturer. Data were normalized using results from the *EGFP* knock-in mouse in the *Cx43* gene (M. Tanaka and S. Itohara, unpublished data), which displays a single copy of *EGFP* in the genome. Then absolute *EGFP* copy numbers in Tg3 ($n = 3$) Tg7 ($n = 3$) and Tg10 ($n = 5$) of *chat-GluR2* mice were calculated as 2.10 ± 0.04, 9.31 ± 0.14 and 16.44 ± 0.67 copies for the *SOD1* control, and 2.13 ± 0.07, 10.20 ± 0.09 and 16.43 ± 1.28 copies for the *CPTI* control, respectively (mean $\pm$ SD). The transgene copy number was thus represented as the mean of these two values.

Electrophysiological recordings

Electrophysiological experiments were performed as previously described (46) using 200–250 μm slices of spinal cord lumbar regions from mice at the postnatal ages of 4–7 days. Whole-cell patch-clamp recordings were performed with motoneurons identified using biocytin-containing Cs-based intracellular solution. To isolate the AMPA current, the extracellular solution contained 20 μM bicuculline, 25 μM D-2-amino-phosphonovaleric acid (D-APV) and 10 μM strychnine, which blocks the GABA, NMDA and glycine receptors, respectively. A glass electrode containing artificial cerebrospinal fluid positioned in the spinal cord was used for synaptic stimulation.

Quantitative analysis of gene expression levels in motoneurons

Spinal cords from 6–8-month-old mice were dissected without fixation, immediately embedded in OCT compound (Tissue-Tek), and frozen in liquid nitrogen. Frozen sections 30 μm thick were processed and stained using 0.01% toluidine blue, and motoneurons in spinal cords were clipped out of sections using laser microdissection (AS LMD, Leica) according to the manufacturer's protocol. About 1000 clipped slices of motoneurons were collected per mouse and subjected to RNA purification using an RNAeasy kit (Qiagen), followed by cDNA synthesis primed with oligo-dT using Superscript II (Gibco-Brl). The gene expression level was examined by Taqman real-time quantitative PCR using probe–primer sets specific to target genes. PCR was performed on an ABI7700 thermalcycler (PE Biosystems) under the manufacturer's recommended conditions, using cDNA derived from 60 (for *GluR2-4* and *ChAT*) or 10 (for *SOD1* and *GAPDH*) clipped slices of motoneurons as templates. Data were normalized with the expression level of *GAPDH*, and presented as a relative expression level compared with the level in the C57BL/6J non-transgenic control mouse.

Animals

Non-transgenic littermates without any transgene are indicated as wt to distinguish them from non-transgenic control mice,

C57BL/6J mice. All data except for Table 1 and Figure 1E are comparisons among littermates. The G1L line of transgenic mice harboring the G93A-mutated human *SOD1* gene (B6SJL-*TgN(SOD1-G93A)*1Gur^{dl}) was purchased from Jackson Laboratories and backcrossed with C57BL/6J mice. We used the littermates generated by crossing male *hSOD1*^{G93A} mice (fourth backcross-generation) with female *chat-GluR2* transgenic mice for all analyses except for a study of disease onset and mortality in Tg10 line (Table 2 and Fig. 2B and C), that involved three S and three GS littermates generated from the third backcrossed *hSOD1*^{G93A} mouse. To determine the day of disease onset, mice were subjected to the rotarod test (47). The retention time on a rotating wheel, the rotarod score, was measured four times per day with a 1-week interval in a blind fashion. Each trial lasted for a maximum of 5 min, during which time the wheel rotates with a linear acceleration from 4 to 40 rpm. The day of disease onset was defined as the day just before the mean retention time of four trials was sequentially shortened to $<80\%$ of the previous time. The end time was defined as the day of death or the day when the mouse was unable to right itself within 30 s (25).

Preparation of crude mitochondrial and post-mitochondrial fractions

Crude mitochondrial and post-mitochondrial fractions were prepared according to an established method (31) with certain modifications. The bovine strum albumin concentration in buffer H was reduced to 0.1%. The spinal cord L1–L5 segments were homogenized in buffer H (1 mg tissue/10 μl buffer H) on ice and centrifuged at 600*g* for 5 min at 4°C to remove unbroken cells. The supernatant was centrifuged at 13 500*g* for 10 min at 4°C, dividing into pellet (crude mitochondrial fraction) and supernatant (post-mitochondrial fraction).

Size-exclusive chromatography

Approximately 200 μg of cytosolic extracts were filtered through Millex-HV PVDF filters (Millipore, 0.45 μm diameter), concentrated with a Vivaspin column (Vivascience, cut-off size, MW 10 000), then resolved on a Superdex200 PC3.2/30 column (linear fractionation range, MW 10 000–600 000; bed volume, 2.4 ml; Pharmacia Biotech) at a flow rate of 40 μl/min in 50 mM sodium phosphate with 150 mM NaCl, pH 7.0. Fractionation started when 800 μl was eluted, and a 30 μl/tube of elutant was collected for a total of 48 tubes. Void volume was determined by the elution profile of dextran blue (2000 kDa). The column was calibrated using gel filtration calibration kits for high- and low-molecular weights (Amersham Bioscience).

Subcellular fractionation

Figure 5A represents a schematic of this procedure. Whole spinal cords were gently homogenized in modified buffer H [0.22 M D-mannitol, 0.07 M sucrose, 20 mM HEPES, pH 7.4, 1 mM EGTA and complete protease inhibitor cocktail (Roche), at 1 mg tissue/10 μl buffer] with a glass–Teflon homogenizer (10 up-and-down strokes) on ice, and centrifuged at 600*g* for 10 min. The supernatants were sequentially centrifuged at 5000*g* for 15 min, 8000*g* for 15 min and 100 000*g* for 1 h, to obtain three pellets (P2, P3 and P4) and the resulting supernatant (S). The pellets generated by the first brief centrifugation were very gently suspended with 2.2 M sucrose containing complete protease inhibitor cocktail (1 mg starting tissue/15 μl), and centrifuged at 40 000*g* for 1 h. The resulting pellets (P1) were rinsed with modified buffer H followed by centrifugation at 12 000*g* for 10 min. The pellets of P1, P2, P3 and P4 were finally resuspended with 1/4, 2, 1/2 and 1/2 volume (μl) of modified buffer H per starting tissue weight (mg), respectively. All centrifugations were performed at 4°C.

Measurement of protein carbonylation

Freshly dissected tissues were sonicated in buffer [50 mM Tris–HCl, pH 7.6, 20 mM $Na_4P_2O_7$, 20 mM sodium fluoride, 1 mM EGTA, 5 mM EDTA, 5 mM DTT and complete protease inhibitor cocktail (Roche), at 1 mg tissue/20 μl buffer] and centrifuged at 500*g* for 5 min. The supernatants were further centrifuged at 100 000*g* for 1 h, and the resulting supernatants were used. The levels of carbonylated proteins in these supernatants were evaluated by measuring absorbance derived from dinitrophenyl (DNP)–hydrazone as previously described (36) with slight modifications. We started with 40 μg of protein and used 6% SOD for a solubilization of the trichloroacetic acid precipitates.

SUPPLEMENTARY MATERIAL

Supplementary Material is available at HMG Online.

ACKNOWLEDGEMENTS

We wish to thank Drs Shin Kwak and Hiroshi Funakoshi for critical reading of the manuscript, Pacific Edit and Ms Bonnie Lee La Madeleine for review prior to submission for publication, Drs Takashi Sakurai, Haruhisa Inoue, Yasuyuki Suzuki and Runa Araya for helpful suggestions, and Ms Sachiko Iita, Yoshie Yoshida (LMD sampling) and Tomoko Yoda (rotarod test) for technical supports. We would also like to thank Drs Stephen F. Heinemann and Yuzuru Imai for kindly donating rat GluR2-4 cDNAs and anti-ubiquitin antibody, respectively. This work was funded by research grants from RIKEN BSI, a Grant-in-Aid for Scientific Research on Priority Area (Advanced Brain Science Project) from the Ministry of Education, Culture, Sports, Science and Technology, Japan, and grants from the Ministry of Health, Labor and Welfare, Japan.

REFERENCES

1. Julien, J.P. (2001) Amyotrophic lateral sclerosis unfolding the toxicity of the misfolded. *Cell*, **104**, 581–591.
2. Rosen, D.R., Siddique, T., Patterson, D., Figlewicz, D.A., Sapp, P., Hentati, A., Donaldson, D., Goto, J., O'Regan, J.P., Deng, H.X. *et al.* (1993) Mutations in Cu/Zn superoxide dismutase gene are associated with familial amyotrophic lateral sclerosis. *Nature*, **362**, 59–62.

3. Gurney, M.E., Pu, H., Chiu, A.Y., Dal Canto, M.C., Polchow, C.Y., Alexander, D.D., Caliendo, J., Hentati, A., Kwon, Y.W., Deng, H.X. *et al.* (1994) Motor neuron degeneration in mice that express a human Cu,Zn superoxide dismutase mutation. *Science*, **264**, 1772–1775.
4. Cleveland, D.W. and Rothstein, J.D. (2001) From Charcot to Lou Gehrig: deciphering selective motor neuron death in ALS. *Nat. Rev. Neurosci.*, **2**, 806–819.
5. Valentine, J.S. and Hart, P.J. (2003) Misfolded CuZnSOD and amyotrophic lateral sclerosis. *Proc. Natl Acad. Sci. USA*, **100**, 3617–3622.
6. Shibata, N., Asayama, K., Hirano, A. and Kobayashi, M. (1996) Immunohistochemical study on superoxide dismutases in spinal cords from autopsied patients with amyotrophic lateral sclerosis. *Dev. Neurosci.*, **18**, 492–498.
7. Bruijn, L.I., Houseweart, M.K., Kato, S., Anderson, K.L., Anderson, S.D., Ohama, E., Reaume, A.G., Scott, R.W. and Cleveland, D.W. (1998) Aggregation and motor neuron toxicity of an ALS-linked SOD1 mutant independent from wild-type SOD1. *Science*, **281**, 1851–1854.
8. Watanabe, M., Dykes-Hoberg, M., Culotta, V.C., Price, D.L., Wong, P.C. and Rothstein, J.D. (2001) Histological evidence of protein aggregation in mutant SOD1 transgenic mice and in amyotrophic lateral sclerosis neural tissues. *Neurobiol. Dis.*, **8**, 933–941.
9. Johnston, J.A., Dalton, M.J., Gurney, M.E. and Kopito, R.R. (2000) Formation of high molecular weight complexes of mutant Cu, Zn-superoxide dismutase in a mouse model for familial amyotrophic lateral sclerosis. *Proc. Natl Acad. Sci. USA*, **97**, 12571–12576.
10. Wang, J., Xu, G. and Borchelt, D.R. (2002) High molecular weight complexes of mutant superoxide dismutase 1: age-dependent and tissue-specific accumulation. *Neurobiol. Dis.*, **9**, 139–248.
11. Wang, J., Slunt, H., Gonzales, V., Fromholt, D., Coonfield, M., Copeland, N.G., Jenkins, N.A. and Borchelt, D.R. (2003) Copper-binding-site-null SOD1 causes ALS in transgenic mice: aggregates of non-native SOD1 delineate a common feature. *Hum. Mol. Genet.*, **12**, 2753–2764.
12. Puttaparthi, K., Wojcik, C., Rajendran, B., DeMartino, G.N. and Elliott, J.L. (2003) Aggregate formation in the spinal cord of mutant SOD1 transgenic mice is reversible and mediated by proteasomes. *J. Neurochem.*, **87**, 851–860.
13. Durham, H.D., Roy, J., Dong, L. and Figlewicz, D.A. (1997) Aggregation of mutant Cu/Zn superoxide dismutase proteins in a culture model of ALS. *J. Neuropathol. Exp. Neurol.*, **56**, 523–530.
14. Shaw, P.J. and Eggett, C.J. (2000) Molecular factors underlying selective vulnerability of motor neurons to neurodegeneration in amyotrophic lateral sclerosis. *J. Neurol.*, **247** (Suppl. 1), I17–I27.
15. Rothstein, J.D., Van Kammen, M., Levey, A.I., Martin, L.J. and Kuncl, R.W. (1995) Selective loss of glial glutamate transporter GLT-1 in amyotrophic lateral sclerosis. *Ann. Neurol.*, **38**, 73–84.
16. Van Damme, P., Leyssen, M., Callewaert, G., Robberecht, W. and Van Den Bosch, L. (2003) The AMPA receptor antagonist NBQX prolongs survival in a transgenic mouse model of amyotrophic lateral sclerosis. *Neurosci. Lett.*, **343**, 81–84.
17. Gurney, M.E., Fleck, T.J., Himes, C.S. and Hall, E.D. (1998) Riluzole preserves motor function in a transgenic model of familial amyotrophic lateral sclerosis. *Neurology*, **50**, 62–66.
18. Bar-Peled, O., O'Brien, R.J., Morrison, J.H. and Rothstein, J.D. (1999) Cultured motor neurons possess calcium-permeable AMPA/kainate receptors. *Neuroreport*, **10**, 855–859.
19. Kruman, II, Pedersen, W.A., Springer, J.E. and Mattson, M.P. (1999) ALS-linked Cu/Zn-SOD mutation increases vulnerability of motor neurons to excitotoxicity by a mechanism involving increased oxidative stress and perturbed calcium homeostasis. *Exp. Neurol.*, **160**, 28–39.
20. Hollmann, M. and Heinemann, S. (1994) Cloned glutamate receptors. *Annu. Rev. Neurosci.*, **17**, 31–108.
21. Sommer, B., Kohler, M., Sprengel, R. and Seeburg, P.H. (1991) RNA editing in brain controls a determinant of ion flow in glutamate-gated channels. *Cell*, **67**, 11–19.
22. Kawahara, Y., Ito, K., Sun, H., Aizawa, H., Kanazawa, I. and Kwak, S. (2004) Glutamate receptors: RNA editing and death of motor neurons. *Nature*, **427**, 801.
23. Naciff, J.M., Behbehani, M.M., Misawa, H. and Dedman, J.R. (1999) Identification and transgenic analysis of a murine promoter that targets cholinergic neuron expression. *J. Neurochem.*, **72**, 17–28.
24. Tateno, M., Fukunishi, Y., Komatsu, S., Okazaki, Y., Kawai, J., Shibata, K., Itoh, M., Muramatsu, M., Held, W.A. and Hayashizaki, Y. (2001) Identification of a novel member of the snail/Gfi-1 repressor family, mlt 1, which is methylated and silenced in liver tumors of SV40 T antigen transgenic mice. *Cancer Res.*, **61**, 1144–1153.
25. Li, M., Ona, V.O., Guegan, C., Chen, M., Jackson-Lewis, V., Andrews, L.J., Olszewski, A.J., Stieg, P.E., Lee, J.P., Przedborski, S. *et al.* (2000) Functional role of caspase-1 and caspase-3 in an ALS transgenic mouse model. *Science*, **288**, 335–339.
26. Zhu, S., Stavrovskaya, I.G., Drozda, M., Kim, B.Y., Ona, V., Li, M., Sarang, S., Liu, A.S., Hartley, D.M., Wu du, C. *et al.* (2002) Minocycline inhibits cytochrome c release and delays progression of amyotrophic lateral sclerosis in mice. *Nature*, **417**, 74–78.
27. Drachman, D.B., Frank, K., Dykes-Hoberg, M., Teismann, P., Almer, G., Przedborski, S. and Rothstein, J.D. (2002) Cyclooxygenase 2 inhibition protects motor neurons and prolongs survival in a transgenic mouse model of ALS. *Ann. Neurol.*, **52**, 771–778.
28. van Gurp, M., Festjens, N., van Loo, G., Saelens, X. and Vandenabeele, P. (2003) Mitochondrial intermembrane proteins in cell death. *Biochem. Biophys. Res. Commun.*, **304**, 487–497.
29. Bezzi, P., Carmignoto, G., Pasti, L., Vesce, S., Rossi, D., Rizzini, B.L., Pozzan, T. and Volterra, A. (1998) Prostaglandins stimulate calcium-dependent glutamate release in astrocytes. *Nature*, **391**, 281–285.
30. Hall, E.D., Oostveen, J.A. and Gurney, M.E. (1998) Relationship of microglial and astrocytic activation to disease onset and progression in a transgenic model of familial ALS. *Glia*, **23**, 249–256.
31. Mattiazzi, M., D'Aurelio, M., Gajewski, C.D., Martushova, K., Kiaei, M., Beal, M.F. and Manfredi, G. (2002) Mutated human SOD1 causes dysfunction of oxidative phosphorylation in mitochondria of transgenic mice. *J. Biol. Chem.*, **277**, 29626–29633.
32. Okado-Matsumoto, A. and Fridovich, I. (2001) Subcellular distribution of superoxide dismutases (SOD) in rat liver: Cu,Zn-SOD in mitochondria. *J. Biol. Chem.*, **276**, 38388–38393.
33. Ookawara, T., Kawamura, N., Kitagawa, Y. and Taniguchi, N. (1992) Site-specific and random fragmentation of Cu,Zn-superoxide dismutase by glycation reaction. Implication of reactive oxygen species. *J. Biol. Chem.*, **267**, 18505–18510.
34. Urushitani, M., Kurisu, J., Tsukita, K. and Takahashi, R. (2002) Proteasomal inhibition by misfolded mutant superoxide dismutase 1 induces selective motor neuron death in familial amyotrophic lateral sclerosis. *J. Neurochem.*, **83**, 1030–1042.
35. Rakhit, R., Cunningham, P., Furtos-Matei, A., Dahan, S., Qi, X.F., Crow, J.P., Cashman, N.R., Kondejewski, L.H. and Chakrabartty, A. (2002) Oxidation-induced misfolding and aggregation of superoxide dismutase and its implications for amyotrophic lateral sclerosis. *J. Biol. Chem.*, **277**, 47551–47556.
36. Andrus, P.K., Fleck, T.J., Gurney, M.E. and Hall, E.D. (1998) Protein oxidative damage in a transgenic mouse model of familial amyotrophic lateral sclerosis. *J. Neurochem.*, **71**, 2041–2048.
37. Liu, R., Althaus, J.S., Ellerbrock, B.R., Becker, D.A. and Gurney, M.E. (1998) Enhanced oxygen radical production in a transgenic mouse model of familial amyotrophic lateral sclerosis. *Ann. Neurol.*, **44**, 763–770.
38. Liu, D., Wen, J., Liu, J. and Li, L. (1999) The roles of free radicals in amyotrophic lateral sclerosis: reactive oxygen species and elevated oxidation of protein, DNA, and membrane phospholipids. *FASEB J.*, **13**, 2318–2328.
39. Clement, A.M., Nguyen, M.D., Roberts, E.A., Garcia, M.L., Boillee, S., Rule, M., McMahon, A.P., Doucette, W., Siwek, D., Ferrante, R.J. *et al.* (2003) Wild-type nonneuronal cells extend survival of SOD1 mutant motor neurons in ALS mice. *Science*, **302**, 113–117.
40. Orrenius, S., McConkey, D.J., Bellomo, G. and Nicotera, P. (1989) Role of Ca^{2+} in toxic cell killing. *Trends Pharmacol. Sci.*, **10**, 281–285.
41. Alexianu, M.E., Ho, B.K., Mohamed, A.H., La Bella, V., Smith, R.G. and Appel, S.H. (1994) The role of calcium-binding proteins in selective motoneuron vulnerability in amyotrophic lateral sclerosis. *Ann. Neurol.*, **36**, 846–858.
42. Carriedo, S.G., Sensi, S.L., Yin, H.Z. and Weiss, J.H. (2000) AMPA exposures induce mitochondrial Ca(2+) overload and ROS generation in spinal motor neurons *in vitro*. *J. Neurosci.*, **20**, 240–250.
43. Rao, S.D., Yin, H.Z. and Weiss, J.H. (2003) Disruption of glial glutamate transport by reactive oxygen species produced in motor neurons. *J. Neurosci.*, **23**, 2627–2633.

44. Bendotti, C., Tortarolo, M., Suchak, S.K., Calvaresi, N., Carvelli, L., Bastone, A., Rizzi, M., Rattray, M. and Mennini, T. (2001) Transgenic SOD1 G93A mice develop reduced GLT-1 in spinal cord without alterations in cerebrospinal fluid glutamate levels. *J. Neurochem.*, **79**, 737–746.
45. Rao, S.D. and Weiss, J.H. (2004) Excitotoxic and oxidative cross-talk between motor neurons and glia in ALS pathogenesis. *Trends Neurosci.*, **27**, 17–23.
46. Suzuki, T., Miura, M., Nishimura, K. and Aosaki, T. (2001) Dopamine-dependent synaptic plasticity in the striatal cholinergic interneurons. *J. Neurosci.*, **21**, 6492–6501.
47. Inoue, H., Tsukita, K., Iwasato, T., Suzuki, Y., Tomioka, M., Tateno, M., Nagao, M., Kawata, A., Saido, T.C., Miura, M. *et al.* (2003) The crucial role of caspase-9 in the disease progression of a transgenic ALS mouse model. *EMBO J.*, **22**, 6665–6674.

THE JOURNAL OF BIOLOGICAL CHEMISTRY
© 2005 by The American Society for Biochemistry and Molecular Biology, Inc

Vol. 280, No. 5, Issue of February 4, pp. 3390–3399, 2005
Printed in U.S.A.

Parkin Phosphorylation and Modulation of Its E3 Ubiquitin Ligase Activity*

Received for publication, July 9, 2004, and in revised form, November 12, 2004
Published, JBC Papers in Press, November 22, 2004, DOI 10.1074/jbc.M407724200

Ayako Yamamoto‡, Arno Friedlein§, Yuzuru Imai¶, Ryosuke Takahashi¶, Philipp J. Kahle‡‖, and Christian Haass‡

From the ‡Laboratory of Alzheimer's and Parkinson's Disease Research, Department of Metabolic Biochemistry, Ludwig Maximilians University, 80336 Munich, Germany, §Roche Center for Medical Genomics, F. Hoffmann-La Roche Ltd. 4070 Basel, Switzerland, and ¶Motor System Neurodegeneration, RIKEN Brain Science Institute, Saitama 351-0198, Japan

Mutations in the *PARKIN* gene are the most common cause of hereditary parkinsonism. The parkin protein comprises an N-terminal ubiquitin-like domain, a linker region containing caspase cleavage sites, a unique domain in the central portion, and a special zinc finger configuration termed RING-IBR-RING. Parkin has E3 ubiquitin-protein ligase activity and is believed to mediate proteasomal degradation of aggregation-prone proteins. Whereas the effects of mutations on the structure and function of parkin have been intensely studied, post-translational modifications of parkin and the regulation of its enzymatic activity are poorly understood. Here we report that parkin is phosphorylated both in human embryonic kidney HEK293 cells and human neuroblastoma SH-SY5Y cells. The turnover of parkin phosphorylation was rapid, because inhibition of phosphatases with okadaic acid was necessary to stabilize phosphoparkin. Phosphoamino acid analysis revealed that phosphorylation occurred mainly on serine residues under these conditions. At least five phosphorylation sites were identified, including Ser^{101}, Ser^{131}, and Ser^{136} (located in the linker region) as well as Ser^{296} and Ser^{378} (located in the RING-IBR-RING motif). Casein kinase-1, protein kinase A, and protein kinase C phosphorylated parkin *in vitro*, and inhibition of casein kinase-1 caused a dramatic reduction of parkin phosphorylation in cell lysates. Induction of protein folding stress in cells reduced parkin phosphorylation, and unphosphorylated parkin had slightly but significantly elevated autoubiquitination activity. Thus, complex regulation of the phosphorylation state of parkin may contribute to the unfolded protein response in stressed cells.

Parkinson's disease (PD)[1] is the second most common neurodegenerative disorder. Parkinsonian symptoms are caused by the progressive loss of dopaminergic neurons in the substantia nigra pars compacta (1). Although more than 90% of PD cases occur sporadically, the study of genetic mutations has offered great insight into the molecular mechanisms of PD (2). After the discovery that mutations in the *PARKIN* gene cause autosomal recessive juvenile parkinsonism (3), parkin mutations have been recognized as the most common cause of hereditary PD and possibly a risk factor for idiopathic PD (4, 5).

The *PARKIN* gene comprises 12 exons and codes for a 465-amino acid protein that is widely expressed, most prominently in muscle and throughout the brain (3). The 52-kDa parkin protein comprises an N-terminal ubiquitin-like domain (aa 1–76), a unique parkin domain (aa 145–232), and two RING (really interesting new gene) fingers (aa 238–293 and 418–449, respectively) flanking an IBR (in-between RING) domain (aa 314–377) at the C terminus. All of these domains appear to be functionally important, because PD mutations cluster in them (6).

Parkin functions in the ubiquitin-proteasome system as an E3 ubiquitin-protein ligase together with the E2 ubiquitin-conjugating co-enzymes UbcH7 or UbcH8 (7–9). Because this function appears to be defective in patients with parkin mutations, the identification of protein substrates is of great importance (6, 10). Parkin substrates include synaptic proteins (the septins CDCrel-1 and CDCrel-2, synaptotagmin XI, and the α-synuclein interactor synphilin-1), PaelR (parkin-associated endothelin-like receptor), cyclin E, α/β tubulin, and the p38 subunit of the aminoacyl-tRNA synthetase complex (9, 11–17). Parkin expression was found to be neuroprotective in *Drosophila* (18) and in cell culture models of dopamine neuron loss (19–22). However, the exact molecular mechanisms of how parkin dysfunction causes PD remain to be elucidated (6, 10).

Post-translational modifications often regulate enzymatic activity. Nitrosylation of parkin was recently found to occur in PD, leading to an inhibition of its ubiquitin ligase activity (23, 24). Here we addressed the question whether phosphorylation of parkin occurred and, if so, by which kinases under what cellular conditions. Parkin was found to be phosphorylated on at least five serine residues. Casein kinase-1 (CK-1), protein kinase A (PKA) and protein kinase C (PKC) were identified as parkin kinases *in vitro*, and inhibition of CK-1 suppressed phosphorylation of parkin in cell lysates. Unfolded protein stress mediated by proteasomal inhibition or endoplasmatic reticulum (ER) stress, but not oxidative stress, reduced the overall phosphorylation of parkin. Unphosphorylated parkin isolated from eukaryotic cells or purified as recombinant fusion protein from bacteria showed a small but significant increase of autoubiquitin ligase activity, compared with parkin phosphorylated *in vivo* and *in vitro*. Thus, we suggest that modulation of the phosphorylation state of parkin has a regulatory role on its E3 ubiquitin ligase activity.

* This work was supported by the German National Genome Research Network, the European Union (N)EUROPARK and APOPIS consortia and by Deutsche Forschungsgemeinschaft Grant SFB596. The costs of publication of this article were defrayed in part by the payment of page charges. This article must therefore be hereby marked "*advertisement*" in accordance with 18 U.S.C. Section 1734 solely to indicate this fact.

‖ To whom correspondence should be addressed. Tel.: 49-89-2180-75480; Fax: 49-89-2180-75415; E-mail: Philipp.Kahle@med.uni-muenchen.de.

[1] The abbreviations used are: PD, Parkinson's disease; aa, amino acid(s); CIP, calf intestinal alkaline phosphatase; CK, casein kinase; ER, endoplasmic reticulum; GST, glutathione *S*-transferase; MALDI, matrix-assisted laser desorption ionization; TOF, time-of-flight; OA, okadaic acid; PDBu, phorbol-12,13-dibutyrate; PKA, protein kinase A; PKC, protein kinase C; E1, ubiquitin-activating enzyme; E2, ubiquitin carrier protein; E3, ubiquitin-protein isopeptide ligase; PVDF, polyvinylidene difluoride; PKB, protein kinase B; ACTH, adrenocorticotropic hormone; RT, reverse transcription.

MATERIALS AND METHODS

Cell Culture, Transfection, and Establishment of Stable Transfectants—HEK293, HEK293T, and SH-SY5Y cells were cultured in Dulbecco's modified Eagle's medium with Glutamax (PAA Laboratories GmbH) supplemented with 10% fetal calf serum for HEK293 cells and HEK293T cells or 15% for SH-SY5Y cells. Cells were transfected using Lipofectamine 2000 Reagent (Invitrogen) or FuGene (Roche Applied Science) according to the supplier's instructions. Stable HEK293 and SH-SY5Y transfectants were selected with 200 or 22.5 μg/ml zeocin, respectively.

Construction of cDNAs—Human full-length parkin was amplified by PCR (all primer sequences are available upon request) using a parkin cDNA construct (a gift from R. Baumeister) and cloned into the XbaI/HindIII restriction sites of pcDNA3.1 zeo(−) (Invitrogen), yielding MYC-parkin.

An additional C-terminal V5 tag was introduced by subcloning into pcDNA6/V5-His (Invitrogen) (MYC-parkin-V5). For mapping the phosphorylation sites, parkin fragments comprising the N terminus (aa 2–144), the N terminus and middle portion (aa 2–293), and the C terminus (aa 294–465) were generated by PCR using the appropriate oligonucleotide primers and cloned into the XbaI/HindIII restriction sites of pcDNA3.1 zeo(−) or the NheI/EcoRI restriction enzyme sites of pcDNA6/V5-His, yielding the constructs MYC-parN(-V5), MYC-parNM(-V5), and MYC-parC(-V5). Serine-to-alanine mutants were generated by mutagenizing respective codons in MYC-parN-V5 or MYC-parC-V5 in two-step PCR.

GST-parkin, GST-parN, and GST-parC were constructed by PCR and cloned into the EcoRI/NotI restriction sites of pGEX-4T-1 (Amersham Biosciences). Serine-to-alanine mutants were generated by mutagenizing the respective codons in GST-parN or GST-parC by two-step PCR. N-terminal FLAG-tagged parkin (FLAG-parkin) and C-terminal FLAG-tagged PaelR (PaelR-FLAG) were described elsewhere (8, 11).

RT-PCR—Total RNA was isolated from both HEK293 cells and stable HEK293 transfectants of parkin under various stresses using peqGOLD RNA Pure (PeQLab). First strand cDNA was synthesized using SuperScript First-Strand Synthesis System for RT-PCR (Invitrogen). RT-PCR was performed using *Taq* DNA polymerase (PeQLab) and the following primers: BiP forward primer, 5′-CCGCATCACGCCGTC-3′; BiP reverse primer, 5′-GGCTCGTTGATGATCCTC-3′.

Immunoprecipitation and Immunoblotting—Cells were harvested 24 h after the transfection and lysed in lysis buffer (10 mM Tris-HCl, pH 7.5, 150 mM NaCl, 1 mM EDTA, and 1% Triton X-100) with proteinase inhibitors (Sigma) on ice for 15 min. Cell lysates were centrifuged at 4 °C at 16,000 × *g* for 20 min. Immunoprecipitations were carried out using protein G-Sepharose (Amersham Biosciences) or protein A-Sepharose, anti-Myc-agarose, anti-FLAG M2-agarose affinity gel (all from Sigma) at 4 °C for 2 h. Immunoprecipitates were washed with lysis buffer three times (or, in the case of radiolabeled samples, six times). Whole cell extracts and immunoprecipitates were separated by SDS-PAGE, and proteins were transferred onto PVDF membrane (Immobilon; Millipore Corp.). Enhanced chemiluminescence detection reagents (Amersham Biosciences) were used to detect immunoblot signals of the following antibodies: 9E10 monoclonal anti-Myc (Developmental Studies Hybridoma Bank, University of Iowa), monoclonal anti-V5 (Invitrogen), monoclonal anti-KDEL against glucose-regulated proteins Grp78 and Grp94 (Stressgen), polyclonal anti-parkin (Cell Signaling), and PRK8 monoclonal anti-parkin (25) (kindly provided by V. Lee).

In Vivo Phosphorylation Assay—Twenty-four h after the transfection, cells were incubated for 45 min in phosphate-free medium (Sigma), and 13–36 MBq of [^{32}P]orthophosphate was added. After 30 min (to label transfected parkin) or 2 h (to label endogenous parkin), 1 μM okadaic acid (OA) was added and incubated at 37 °C for 1 h. The conditioned medium was aspirated, and the cell monolayer washed twice with ice-cold phosphate-buffered saline. Cells were lysed on ice with lysis buffer, and immunoprecipitations were performed as above. Immunoprecipitates were separated by SDS-PAGE and transferred onto PVDF membrane. Autoradiography was carried out to visualize radiolabeled proteins.

Matrix-assisted Laser Desorption Ionization Time-of-flight (MALDI-TOF) Mass Spectrometry—Phosphorylation of transfected MYC-parkin fragments was induced with OA, and MYC immunoprecipitates were subjected to SDS-PAGE. Colloidal blue-stained bands of interest were in-gel digested with endoproteinase Lys-C as described (26). After overnight digestion, about 1 μl was mixed with 1 μl of saturated α-cyano-cinnamic acid in 50% acetonitrile, 0.1% trifluoroacetic acid in water and applied to the MALDI target. The samples were analyzed with a Bruker Daltonics (Bremen, Germany) Ultraflex TOF/TOF mass spectrometer.

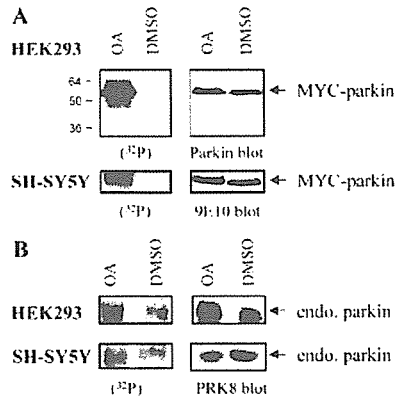

FIG. 1. **Parkin is phosphorylated both in HEK293 cells and SH-SY5Y cells.** *A*, HEK293 cells (*upper panels*) and SH-SY5Y cells (*lower panels*) stably expressing MYC-parkin were labeled with [^{32}P]orthophosphate in the presence or absence of OA, and then cell lysates were immunoprecipitated with 9E10. Proteins separated by 12% SDS-PAGE were transferred onto PVDF membrane. Autoradiography was carried out in order to visualize phosphorylated parkin (*left panels*). Afterward, blots were probed with polyclonal anti-parkin or 9E10 anti-Myc (*right panels*). *B*, endogenous parkin in HEK293 cells (*upper panels*) and SH-SY5Y cells (*lower panels*) was labeled with [^{32}P]orthophosphate and immunoprecipitated with polyclonal anti-parkin. After the autoradiography (*left panels*), blots were probed with PRK8 monoclonal anti-parkin (*right panels*). *DMSO*, Me_2SO.

An acceleration voltage of 25 kV was used. Calibration was internal to the samples with des-Arg-bradykinin and ACTH-(18–38) (both peptides purchased from Sigma).

Nanoelectrospray Ionization Tandem Mass Spectrometry—In order to identify which of the three possible serines was phosphorylated in the parkin peptide obtained after digestion with endoproteinase Lys-C with a monoisotopic mass of 1568.75 Da, this proteolytic product was subjected to nanoelectrospray ionization tandem mass spectrometry on a QSTAR Pulsar I quadrupole TOF tandem mass spectrometer (Applied Biosystems/MDS-Sciex, Toronto, Canada) equipped with a nanoelectrospray ion source (Proxeon, Odense, Denmark) as described (27).

Dephosphorylation by Alkaline Phosphatase—HEK293 cells and SH-SY5Y cells were transiently transfected with MYC-parkin-V5 and various portions of parkin (MYC-parN-V5, MYC-parNM-V5, and MYC-parC-V5). Twenty-four h after the transfection, 1 μM OA was added, and cells were incubated for 1 h. Immunoprecipitation using anti-Myc-agarose conjugate (Sigma) was performed. Immunoprecipitates were incubated at 37 °C for 1 h with or without calf intestinal alkaline phosphatase (CIP) (New England Biolabs) according to the supplier's manual. Reactions were terminated by adding 2× SDS sample buffer and analyzed by immunoblot.

Phosphoamino Acid Analysis—Phosphoamino acid analysis was performed using the method by Jelinek and Weber (28). After electroblotting radiolabeled proteins onto PVDF membrane, bands were excised and hydrolyzed using 6 N HCl at 100 °C for 90 min. After centrifugation, supernatants were dried in a SpeedVac concentrator. Pellets were dissolved in pH 2.5 buffer (5.9% glacial acetic acid, 0.8% formic acid, 0.3% pyridine, and 0.3 mM EDTA) and spotted onto thin layer chromatography plates (Merck) together with unlabeled phosphoamino acid markers (1 μg each of Ser(P), Thr(P), and Tyr(P); Sigma). One-dimensional high voltage electrophoresis was performed at 20 mA for 50 min. Radioactive phosphoamino acids were identified by autoradiography and co-migration with the ninhydrin-stained standards.

In Vitro Phosphorylation Assays—Recombinant rat CK-1 δ, recombinant α-subunit of human CK-2 and recombinant human Akt1/PKB protein kinase were used for *in vitro* phosphorylation assays according to the supplier's instructions (Cell Signaling). The catalytic subunit of PKA purified from bovine heart (gift from V. Kinzel) was used in a buffer containing 20 mM Tris, pH 7.5, 5 mM magnesium acetate, and 5 mM dithiothreitol. PKC purified from rat brain (Biomol) was used in a similar buffer to PKA supplemented with 1 μM phorbol-12,13-dibutyrate (PDBu), 0.5 mM $CaCl_2$, and 100 μg/ml phosphatidylserine under mixed micellar conditions. Fusion proteins GST-parkin, GST-parN, GST-parC, and various serine-to-alanine mutations in GST-parN or GST-parC were used as substrates. The reaction was started by adding 10 μM [γ-^{32}P]ATP (250 μM [γ-^{32}P]ATP in the case of Akt1/PKB) and allowed to proceed for 30 min at 30 °C.

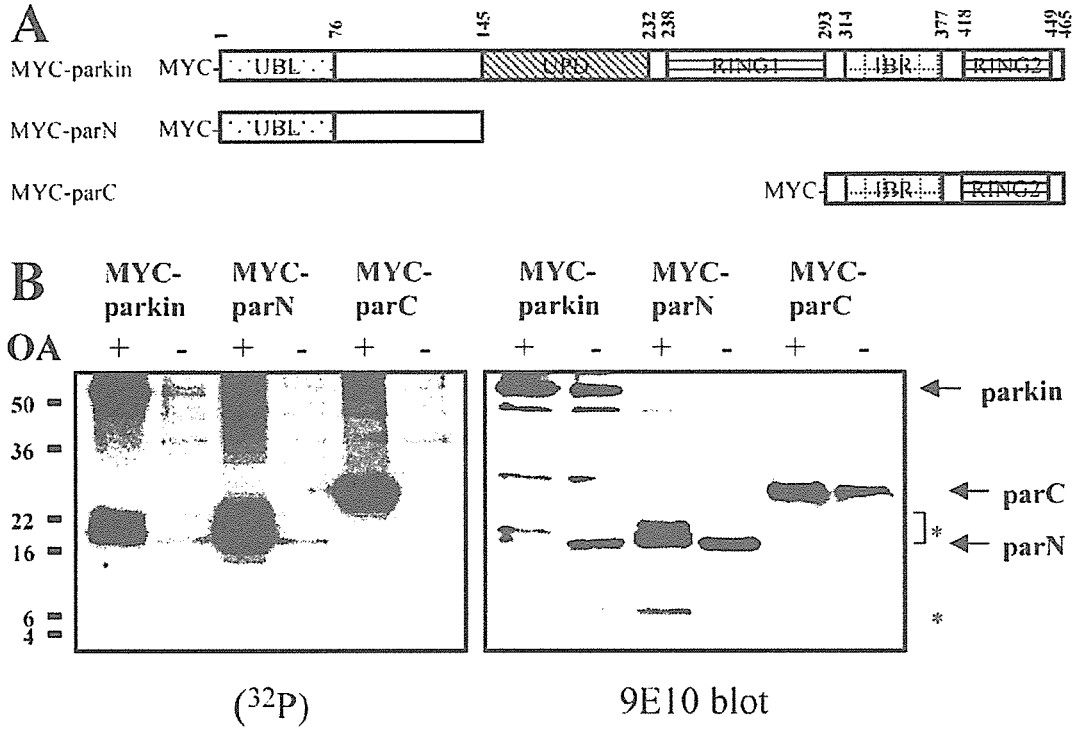

FIG. 2. **Both N terminus and C terminus of parkin are phosphorylated.** *A*, schematic representation of MYC-parkin, MYC-parN, and MYC-parC, which were used to establish stable transfectants in HEK293 cells. *B*, the experimental procedure was followed as described in Fig. 1*A*. Autoradiography was carried out in order to visualize phosphorylated parkin (*left panel*). Afterward, the immunoblot was probed with 9E10 anti-Myc (*right panel*). *, cleaved forms of MYC-parkin.

Alternatively, cell lysates were used to phosphorylate fusion proteins of GST carrying parkin, parN, and parC. HEK293 cells were lysed in a buffer containing 20 mM Tris, pH 7.5, 5 mM magnesium acetate, 5 mM dithiothreitol, and 0.5% Triton X-100. In case of PKC, 0.5 mM $CaCl_2$, 1 μM PDBu, and 100 μg/ml phosphatidylserine were added. After centrifugation at 14,000 × *g* at 4 °C for 10 min, GST-parkin, GST-parN, GST-parC, or various serine-to-alanine mutants were added to supernatants. Phosphorylation reactions were started by adding [γ-^{32}P]ATP and allowed to proceed at 30 °C for 30 min in the presence of 4 μM OA and in the presence or absence of 5 μM hymenialdisine (donated by L. Meijer), 5 μM H-89 (Biomol), or 5 μM GF 109203X (Biomol). After the reaction, precipitations with glutathione-Sepharose (Amersham Biosciences) were carried out at 4 °C for 2 h. Precipitates were washed four times with phosphate-buffered saline and eluted by 2× SDS sample buffer.

In Vitro Ubiquitination Assay—FLAG-parkin was transfected into HEK293T cells. Twenty-four h after the transfection, 1 μM OA was added to cells and incubated for 50 min. Cells were harvested and lysed in lysis buffer. Alternatively, GST-parkin immobilized on glutathione-Sepharose, which was phosphorylated by CK-1, PKA, or PKC was used. Immunoprecipitates using anti-FLAG M2-agarose (Sigma) or immobilized phosphorylated GST-parkin were washed three times with lysis buffer and once with ubiquitination buffer (50 mM Tris-HCl, pH 7.4, and 5 mM $MgCl_2$). One mM dithiothreitol, 2 mM ATP, 100 ng of E1 (AFFINITI), 2 μg of UbcH7 (AFFINITI or MBL) and 5 μg of ubiquitin biotinylated using the EZ-Link Sulfo-NHS biotinylation kit (Pierce) were added to the immunoprecipitates. The reactions were conducted at 30 °C for 90 min and terminated by adding 2× SDS sample buffer. Reaction mixtures were resolved by 10% SDS-PAGE, and immunoblot was carried out using anti-FLAG M2 monoclonal antibody (Sigma) or streptavidin-peroxidase polymer (Sigma). Autoubiquitination (biotinylated) of parkin was quantified by densitometric scanning of the streptavidin-peroxidase developed blots. Image analysis was done using NIH Image version 1.62 (available on the World Wide Web at rsb.info.nih.gov/nih-image).

RESULTS

Parkin Is Constitutively Phosphorylated at the N Terminus and the C Terminus—In order to examine whether or not parkin is phosphorylated, we carried out *in vivo* phosphorylation assays. Stable HEK293 and SH-SY5Y transfectants expressing MYC-parkin were labeled with [^{32}P]orthophosphate. Phosphorylation was stabilized with OA, which inhibits phosphoprotein phosphatase 1, 2A, and 2B. Analysis of Myc-immunoprecipitated parkin by autoradiography revealed that full-length MYC-parkin undergoes phosphorylation both in HEK293 cells and SH-SY5Y cells (Fig. 1*A*). OA treatment also increased the [^{32}P]orthophosphate incorporation into endogenous parkin present at low levels in HEK293 and SH-SY5Y cells (Fig. 1*B*).

To assess which portion of parkin is phosphorylated, we generated Myc-tagged N-terminal parkin (aa 2–144) (parN) and C-terminal parkin (aa 294–465) (parC) constructs (Fig. 2*A*) and established their stable transfectants. Stable transfectants from the middle portion of parkin (aa 145–293) could not be established, possibly due to folding difficulties of the polypeptide. Both N-terminal and C-terminal parkin fragments were phosphorylated (Fig. 2*B*). We also noted in the anti-Myc immunoprecipitates phosphorylated protein bands that were possibly cleavage products derived from full-length parkin (29–31) and resembled the parN fragments in terms of $^{32}PO_4$ incorporation and band shift. Retarded electrophoretic motility of the phosphorylated bands was evident for N-terminal parkin fragments, whereas such a mobility shift was not observed in parC (Fig. 2*B*). Thus, parkin is phosphorylated in both N terminus (with mobility shift) and C terminus (without mobility shift).

In order to further prove that parkin is phosphorylated and the observed electrophoretic motility shift of parN is caused by the covalent incorporation of phosphate, parkin immunoprecipitates were dephosphorylated with CIP. For this set of experiments, HEK293 and SH-SY5Y cells were transiently transfected with double-tagged MYC-parkin-V5, MYC-parN-V5, and MYC-parC-V5 (Fig. 3*A*). Transiently transfected cells were treated with OA and lysed, and the washed Myc-agarose immunoprecipitates were incubated with or without CIP. Then samples were subjected to 10–15% Tris/glycine gel electro-